Depolarization and Second Harmonic Generation in Photonic Crystal Slabs

L.T.H. van Dellen

Master Thesis

Leiden University

2013

Contents

Introduction

Photonic crystals are attractive optical materials for controlling and manipulating the flow of light. Photonic crystals are periodic optical nanostructures and can be fabricated for one, two, or three dimensions. In the present work we will present the results of measurements on a two-dimensional photonic crystal which is a slab of dielectric material with a square lattice of holes.

Photonic crystal slabs have the ability to partially confine propagating light inside by total internal reflection. A resonance that couples incident light to the confined mode and vice versa is created due to the lattice of periodic holes. The holes allow interaction with the outside light field and the guided modes are called leaky modes.

Part 1 of this thesis describes the results of linear transmission measurements of the photonic crystal slab between parallel and crossed polarizers. In this part the presence of leaky modes is mapped as a function of crystal orientation relative to the input light wavevector. We identify resonances in the optical and near-infrared part of the transmission spectrum when the polarizations of the input optical field and output optical field are in parallel. Contrary to theoretical predictions for a perfect lattice we also found resonances when the output field has a polarization rotated 90° relative to the input field.

The photonic crystal slab creates a means for light to resonate inside slab of dielectric material and this leads to an enhanced interaction between light and matter. Therefore, non-linear effects such as second and higher harmonic generation, difference frequency and parametric down-conversion are expected to be greatly enhanced.

Part 2 of this thesis describes the measurement results of second harmonic generation in the photonic crystal. The second harmonic generation is measured as a function of crystal orientation and in different polarization configurations. The second harmonic generation is shown to be greatly enhanced (by a factor up to 10^4) when the frequency of the input light and resonances in the crystal are equal. There are also indications that the resonances at the double frequency enhance the output of second harmonic light.

Part 1

Crossed polarizers

1 Experiment

In all linear transmission experiments described here we use the setup depicted in Fig. 1.1. The white light source is an incandescent halogen lamp, which is connected to a 50 μm multi-mode fiber. The fiber output is imaged onto the sample with 1.5× magnification, i.e. the illuminated area has diameter ~ 75 μm. Using an aperture (3 mm) we limit the beam divergence to a numerical aperture NA < 0.025. The incident light is linearly polarized with a Glan-Thomson polarizing beam splitter. Another such polarizer is used as an analyzer. We set polarizer and analyzer individually to s or p*, thus providing parallel ($s \to s$, $p \to p$) and crossed ($s \to p$, $p \to s$) polarization configurations. Various spectrometers can be attached to the collecting 600 μm multi-mode fiber in order to measure the transmittance. For the visual to near-infrared part of the spectrum (650 nm $\leq \lambda \leq$ 900 nm) we use a silicon CCD array spectrometer (Ocean Optics USB2000) with $\sim$ 1.5 nm spectral resolution. The infrared spectrum (900 nm $\leq \lambda \leq$ 1700 nm) is collected with an InGaAs array spectrometer (Ocean Optics NIR512) with $\sim$ 3 nm resolution.

We perform the experiments on a photonic crystal of $Al_{0.35}Ga_{0.65}As$ with a square lattice of holes with radius of $\sim$ 150 nm and lattice constant or pitch $a = 820$ nm. The lattice of holes is fabricated using e-beam lithography and reactive ion etching techniques. The slab thickness is $\sim$ 150 nm and of size $\sim 300 \times 300$ μm^2. The photonic crystal is placed on a transparent gel substrate with index $n_{\text{gel}} = 1.4$ which in turn sticks to a glass

*s (senkrecht) and p denote the polarizations perpendicular to and parallel to the plane of refraction, respectively.

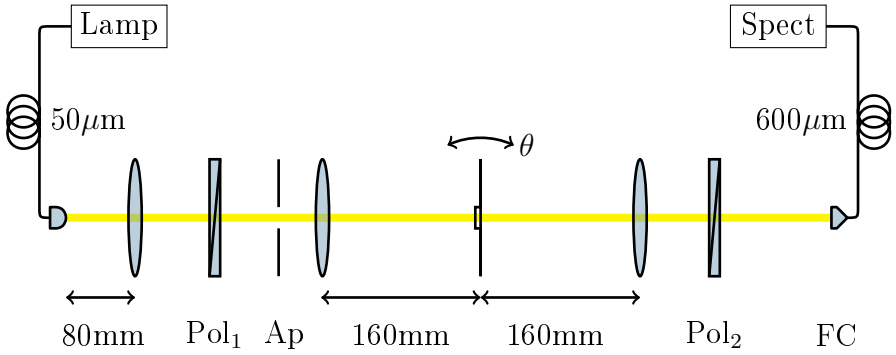

Figure 1.1: The transmission spectrometer setup using a halogen light source, two polarizers and a rotation stage. Details of the sample mount and translation stages are omitted.

microscope slide [1]. In this asymmetric sample we have chosen to perform the transmission measurements through gel-pc-air (and not vice versa). The microscope slide is cut and attached to a ring mount which allows manual alignment of the orientation of the photonic crystal axis relative to the vertical rotation axis. We orient the sample so that the parallel component of the wavevector of the incident light is either along the ΓX or ΓM symmetry directions of the photonic lattice. To align the parallel component of the wavevector along the symmetry directions, we check the diffraction pattern of the lattice formed by a laser pointer operating at a wavelength of 532 nm. Two horizontal translation stages allow centering of the sample mount to the rotation axis. A motorized rotation stage allows automation of transmission experiments as a function of angle of incidence. The ring mount is made thin to allow for transmission measurements at oblique angles up to ±50° from normal incidence. Two more horizontal translation stages allow alignment of the rotation axis to intersect with the optical axis and focal point. A vertical translation stage allows alignment of the sample to the focal point.

We choose to limit the transmission measurements to angles of incidence between −50° and 50° along the ΓX and ΓM symmetry directions of the square lattice. The parameters and configurations used are summarized in Table 1.1.

A reference spectrum is measured for each configuration at the beginning of the measurement series. This reference spectrum is measured by translating the photonic crystal is out of the beam path. For configurations with crossed polarizers we choose the corresponding parallel configuration by

Spectral range	NIR, visual
Crystal orientation	ΓX, ΓM
Polarization	$s \to s$, $p \to p$, $s \to p$, $p \to s$
Transmission direction	gel→pc→air
Angle of incidence	$-50° < \theta < 50°$ (0.25° stepsize)

Table 1.1: Summary of configuration parameters used in the linear transmission experiments. In total, a collection of 6336 spectra are measured.

rotating only the analyzer.

The integration time is selected using the reference spectrum, typically $\tau \approx 1$ s for visual and $\tau \approx 20$ s for NIR spectra. For crossed polarizers the integration time is multiplied to increasethe signal and enhance the signal-to-noise ratio. Typically, the integration time is increased $\times 20$ for ΓM and $\times 40$ for ΓX directions. The transmission spectrum is then calculated using the equation

$$T(\lambda) = \frac{I(\lambda) - I_0(\lambda)}{I_R(\lambda) - I_{R0}(\lambda)} \frac{\tau_R}{\tau} \tag{1.1}$$

with raw spectral intensities $I(\lambda)$, $I_0(\lambda)$, $I_R(\lambda)$, $I_{R0}(\lambda)$ for sample, sample dark, reference, and reference dark respectively. The integration times are denoted as τ and τ_R for the measurement and the reference, respectively.

2 Results and discussion

2.1 Parallel polarizers

Figure 1.2 shows the measured transmission of a square lattice photonic crystal slab with a pitch of $a = 820$ nm. Transmission is shown as a grayscale plot as a function of in-plane wavevector $k_{||}$ (horizontal axis) and dimensionless frequency ω (vertical axis). The four panels correspond to different configurations of the experiment.

The dimensionless frequency units on the vertical axis make explicit that all features in the measured transmission spectra are related to the periodic structure and scale with the pitch a. For similar reasons the pitch a also appears in the units of $k_{||}$. To convert from a wavelength λ to dimensionless frequency is straightforward by using $\omega = \frac{a}{\lambda}$, e.g. the dimensionless frequency of 1 corresponds to a wavelength $\lambda = 820$ nm for the sample used in this experiment. The wavevector $k_{||}$ is the component of the incident wavevector along the surface, i.e. $k_{||} = k \sin\theta = \frac{\omega}{c} \sin\theta$.

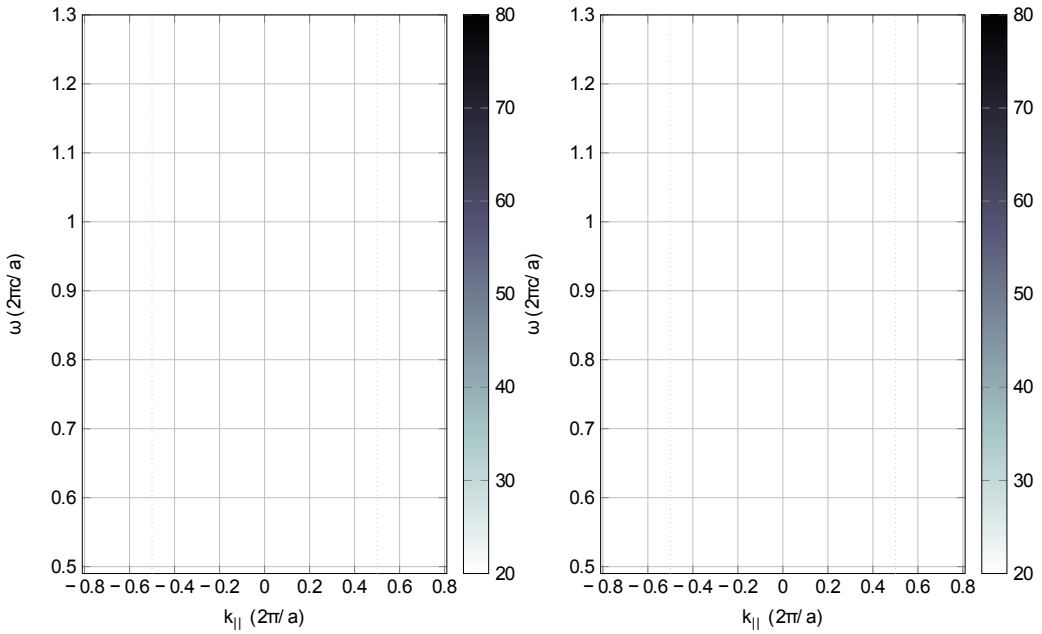

(a) ΓX $s \to s$ (b) ΓX $p \to p$

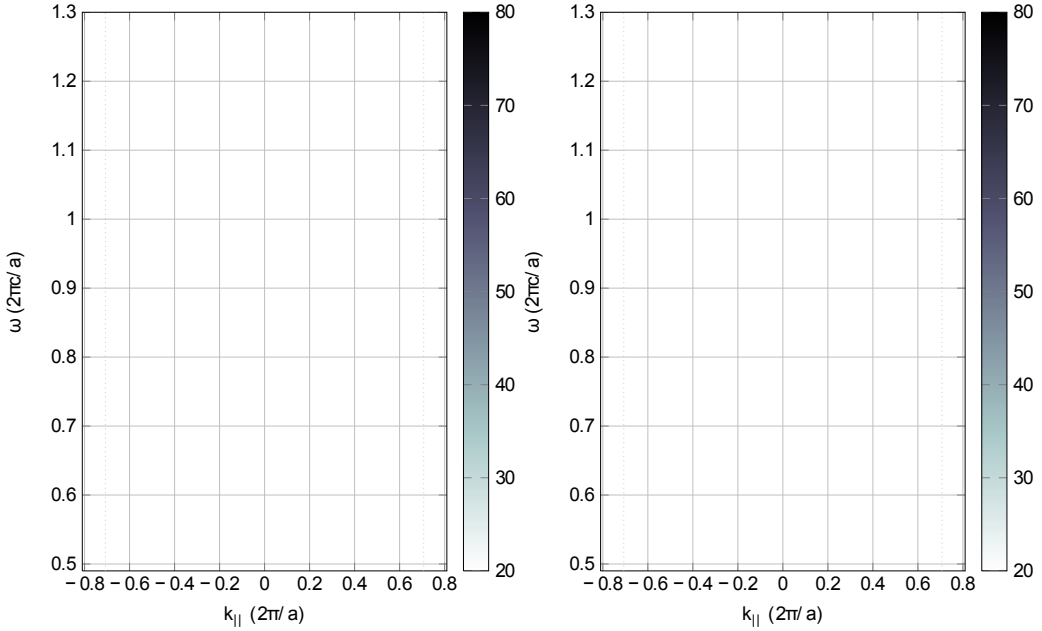

(c) ΓM $s \to s$ (d) ΓM $p \to p$

Figure 1.2: Measured transmission of a square lattice photonic crystal slab with a pitch of $a = 820$ nm. Transmission is shown as a grayscale plot as a function of in-plane wavevector $k_{||}$ (horizontal axis) and dimensionless frequency ω (vertical axis). The four panels correspond to different configurations of experiment. In (a), (b) $k_{||}$ is oriented along crystal axis ΓX and in (c), (d) along the ΓM-axis. The crystal is sandwiched between polarizers in s-orientation (a), (c) or in p-orientation (b), (d).

For all configurations we immediately observe sharp features on top of a slowly varying background visible as bright lines in Fig. 1.2. The ω and $k_{||}$ dependence of the dispersive features represent an experimental measurement of the photonic band structure. [2] More on the interpretation of the structure will be given after the description of the measured data, see Section 2.3 on the slab waveguide model.

Measurements are presented for $k_{||}$ oriented along the two main symmetry directions of the square lattice; the ΓX direction corresponds to the $(1, 0)$ direction and the ΓM corresponds to the $(1, 1)$ direction in reciprocal space. The advantage of these plots is that straight lines in the diagram correspond to constant refractive index.

The diagrams show mirror symmetry about normal incidence ($k_{||} = 0$). Only where signal quality diminishes (at large angles), this symmetry becomes harder to recognize. Additional mirror symmetry for the resonant frequencies can also be found at the edges of the Brillouin zone at $k_{||} = \pm\frac{\pi}{a}$ in the ΓX direction and with more difficulty at $k_{||} = \pm\frac{\pi}{a}\sqrt{2}$ in the ΓM direction.

Fano resonance

Figure 1.3 displays two transmission spectra in the selected frequency range of $0.52 - 0.56\ c/a$, corresponding to 1577 – 1464 nm. It shows in detail one of the resonances found in the transmission spectra of ΓM configurations $s \rightarrow s$ and $p \rightarrow p$. The data displayed here is part of the data displayed in the dispersion diagrams of Fig. 1.2(c) and (d). In both measurements, the angle of incidence is $-2°$, which corresponds to a line of data with slope $k_{||} = -0.035 \cdot \omega/c$ in Fig. 1.2.

The resonance in Fig. 1.3 is not a symmetric Lorentzian line-shape, but has a distinct dispersive nature that can be described by the line-shape of a Fano resonance. [3, 4] The Fano line-shape finds its origin in the interference of a discrete mode and a continuum. [5] The inset in Fig. 1.3 depicts these two channels schematically (not to scale). One channel (1) is the (non-resonant) directly transmitted light through the photonic crystal which can be seen as a thin film. The second channel (2) is a resonant channel; the incident light diffracts off the periodic structure into a guided mode of the slab. The light propagates for some time in the plane of the crystal before it diffracts outward. The interference of the direct channel and the indirect resonant channel manifests itself as an asymmetric line-shape in the spectrum near the resonant frequency. For the resonance depicted in Fig. 1.3, the spectrum shows a minimum just below the resonance frequency, a steep slope at resonance and a maximum just above the resonance frequency.

The Fano line-shape in the transmission spectra can be described by

$$T(\omega) = \left| c_1 + c_2(\omega - \omega_0) - \frac{c_3 + ic_4}{i(\omega - \omega_0) + \gamma} \right|^2 . \tag{1.2}$$

Here we approximate the field of the direct channel as a linearly varying background (coefficients c_1 and c_2). The resonant channel is described by four parameters. The Fano resonance is centered at frequency ω_0 and has spectral width γ (related to the life time of the resonance). The coefficients c_3 and c_4 determine the amplitude and phase of the field. For positive values of c_3 the minus sign in Eq. 1.2 gives a Fano line-shape with a minimum at $\omega < \omega_0$ and a maximum at $\omega > \omega_0$.

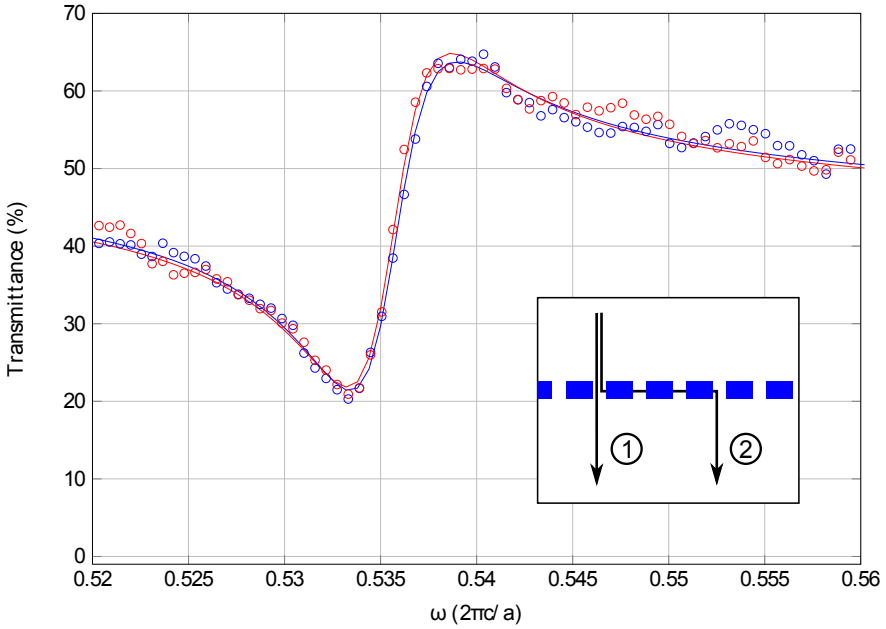

Figure 1.3: Detail of the resonances found in transmission spectra of ΓM configurations with $s \to s$ (blue) and $p \to p$ (red), measured at $-2°$ angle of incidence. The dots show the measured data. Lines through the data are fits to the Fano lineshape given by Eq. 1.2 (see text). The inset shows a schematic drawing of the direct (1) and indirect (2) contributions to the transmission. Interference between these contributions leads to the Fano line-shape.

The lines through the data in Figure 1.3 are fits to the Fano line-shape given by equation 1.2. Table 1.2 displays the parameters and their values for the fits. Note that the ω_0 and γ values are not exactly equal for the two fitted curves, but the difference is below the statistical error (2σ bounds).

Therefore, these two fitted curves do not have a significant difference. Furthermore, we note that the resolution of the spectrometer (3 nm) at this wavelength ($\approx$ 1500 nm) is sufficient to measure the spectral width γ of these Fano line-shapes as $\gamma/\omega_0 = 0.0027/0.5356 \approx 2.52 \cdot (3/1500)$.

	$s \rightarrow s$ & $p \rightarrow p$
ω_0	0.5356 ± 0.0001
γ	0.0027 ± 0.0001
c_1	6.88 ± 0.02
c_2	-4.4 ± 0.6
c_3	0.033 ± 0.002
c_4	-0.0083 ± 0.0003

Table 1.2: Fit parameters and their values for the Fano line-shape fits displayed in Fig. 1.3. Only one column with the average value is listed as the values for $s \rightarrow s$ and $p \rightarrow p$ are within each other's 95% confidence bounds. The values have dimensionless units $(2\pi c/a)$

2.2 Crossed polarizers

The Fano model as introduced in Eq. 1.2 contains a direct and a resonant contribution. The direct contribution is related to the Fresnel transmission coefficients of the thin film and can be switched off by investigating an experimental configuration with crossed polarizers. Figure 1.4 shows the measured transmission of the photonic crystal between crossed polarizers.

The experimental results in Fig. 1.4 immediately show that the resonance does not vanish but remains visible as a symmetric feature on top of the zero-valued background signal. We recognize that the Fano line-shape is reduced to a Lorentzian line-shape. The Lorentzian transmission function can be described by Equation 1.3:

$$T(\omega) = \left| \frac{c_3 + ic_4}{i(\omega - \omega_0) + \gamma} \right|^2 = \frac{A^2}{1 + ((\omega - \omega_0)/\gamma)^2}. \tag{1.3}$$

This equation can be compared to the Fano transmission function of Eq. 1.2. Since the background has vanished, so do the coefficients c_1 and c_2. Also, the phase between direct and indirect channel becomes irrelevant and the complex amplitude $c_3 + ic_4$ is reduced to a simple amplitude coefficient A^2. The resonance frequency ω_0 and its width γ remain in place.

The Lorentzian transmission function is fitted to the spectrum measured with crossed polarizers as shown in Fig. 1.4 and the values for the fit parameters are presented in Table 1.3. The Lorentzian fits well to the data.

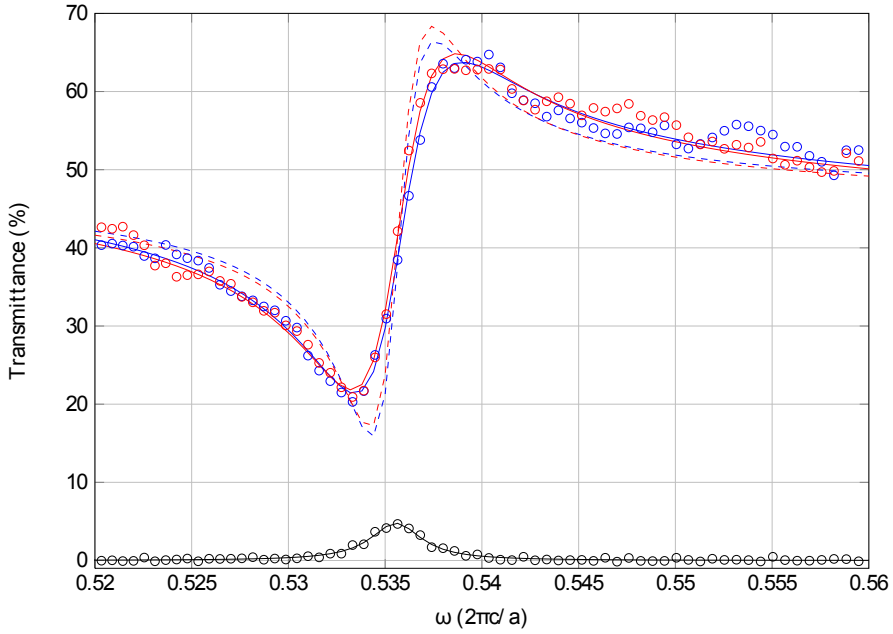

Figure 1.4: Detail of the dispersive feature found in transmission spectra of ΓM configurations with $s \to s$ (blue), $p \to p$ (red) and crossed polarization $s \to p$ (black), measured at -2° angle of incidence. The dots show the measured data. The black data is multiplied $10\times$ for visibility. Red and blue lines through the data are fits of the Fano lineshape given by Eq. 1.2. The black line through the data is a fit to the Lorentzian line-shape given by Eq. 1.3. Dashed lines are Fano line-shape fits to the red and blue data, but the values for ω_0 and γ are taken from the Lorentzian fit (see text).

Even though the transmittance is low (fitted maximum intensity $A^2 < 0.5\%$), the signal is clearly visible above the background. Note that we used 20× multiplied integration times (see Eq. 1.1) to measure this small signal.

	$s \rightarrow p$
ω_0	0.5356 ± 0.0001
γ	0.0016 ± 0.0001
A^2	0.477 ± 0.027

Table 1.3: Fit parameters and their values (with 95% confidence bounds) for the Lorentz line-shape fits displayed in Fig. 1.4.

We compare the parameters ω_0 and γ of the Fano line-shape with the Lorentzian line-shape. We find that both spectral features have the same center frequency ω_0. The spectral width γ, however, is significantly (1.7×) larger for the Fano line-shape than for the Lorentzian (0.0027 vs 0.0016). Emphasizing that this difference is relevant, the dashed lines in Fig. 1.4 show fits of the Fano line-shapes to the data again, but having the parameters ω_0 and γ fixed and set equal to the Lorentzian fit results. Clearly this results in a much sharper spectral feature that what is observed in the experiment. At this point a clear physical picture of what causes this difference is missing and beyond the scope of this thesis. In the remainder of this chapter we will focus on the dispersion of the frequencies ω_0 as a function of $k_{||}$. To this end we will use both data with parallel polarizers and with crossed polarizers.

Dispersion

The dispersion diagram in Figure 1.5 shows the measured transmission of the square lattice photonic crystal slab with a pitch of $a = 820$ nm when sandwiched between 90° crossed polarizers. Transmission is shown as a grayscale plot as a function of in-plane wavevector $k_{||}$ (horizontal axis) and dimensionless frequency ω (vertical axis). The four panels correspond to different configurations in the experiment. In (a), (b) $k_{||}$ is oriented along the ΓX symmetry direction and in (c), (d) along the Γ symmetry direction. Polarizers are oriented either $s \rightarrow p$ (a), (c) or $p \rightarrow s$ (b), (d). The transmission is calculated using Eq. 1.1.

Immediately we notice that the single feature displayed in Fig. 1.4 is not the only resonance that remains visible when crossing the polarizers. Many resonances, throughout the dispersion diagram in Fig. 1.5, show a visible Lorentzian response in measurements with crossed polarizers while there are Fano line-shapes when measuring with parallel polarizers (Fig. 1.2). Especially in the ΓM configuration, the visibility of resonances is clear. In fact,

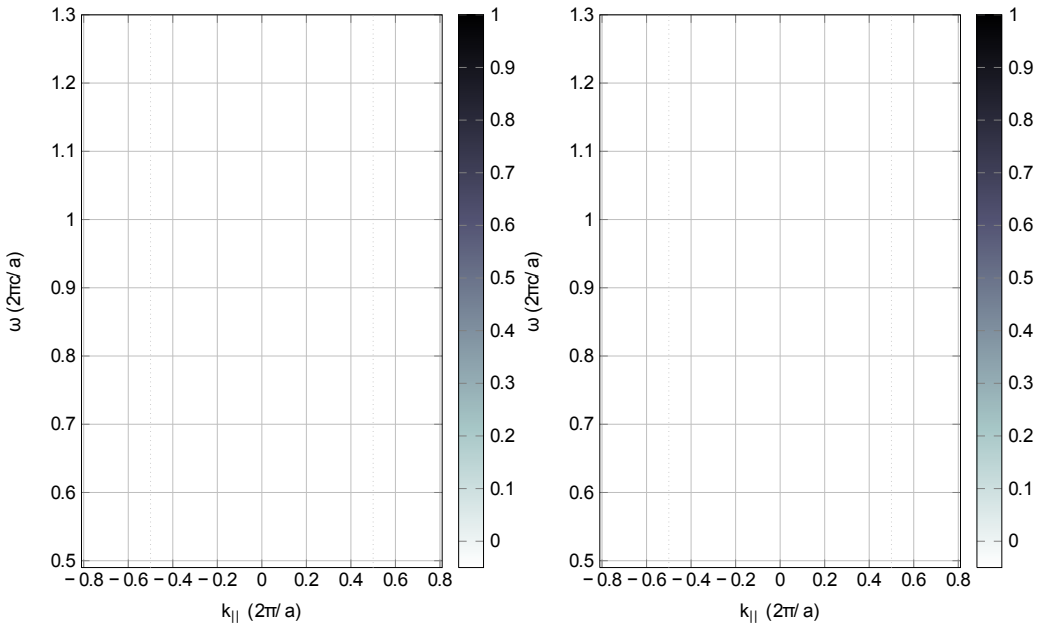

(a) ΓX $s \rightarrow p$ (b) ΓX $p \rightarrow s$

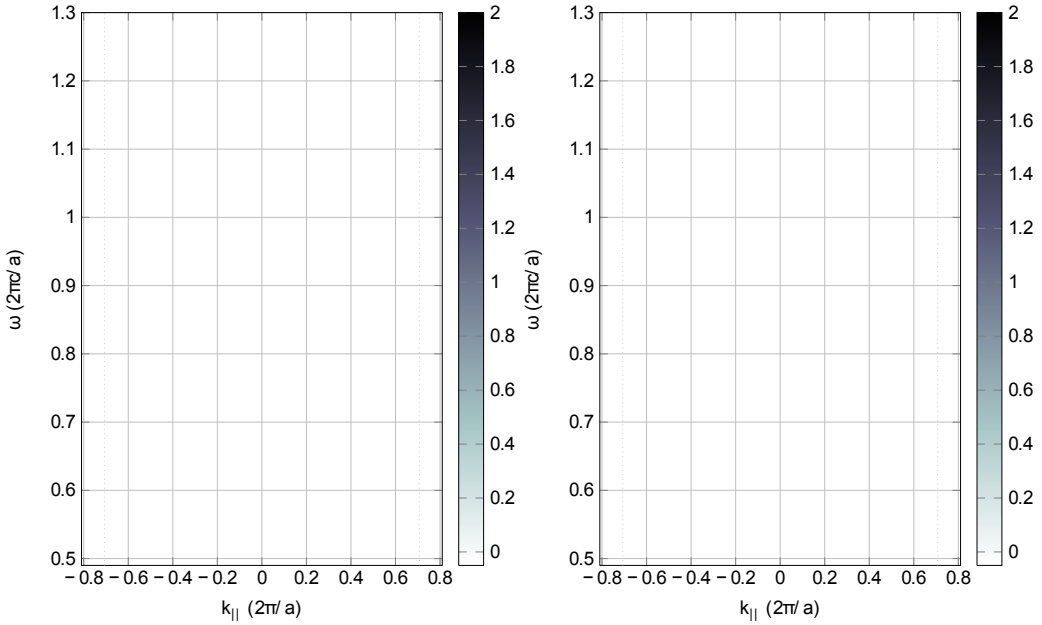

(c) ΓM $s \rightarrow p$ (d) ΓM $p \rightarrow s$

Figure 1.5: Measured transmission of a square lattice photonic crystal slab with a pitch of $a = 820$ nm sandwiched between 90° crossed linear polarizers. Transmission is shown as a grayscale plot as a function of in-plane wavevector $k_{||}$ (horizontal axis) and dimensionless frequency ω (vertical axis). The four panels correspond to different configurations of experiment. In (a),(b) $k_{||}$ is oriented along crystal axis ΓX and in (c),(d) along the ΓM-axis. Polarizers are oriented $s \rightarrow p$ in (a),(c) or $p \rightarrow s$ (b),(d). The transmission is calculated using Eq. 1.1.

resonances from the two parallel configurations $s{\rightarrow}s$ and $p{\rightarrow}p$ are simultaneously visible in each crossed polarized configuration. The diagrams of $s{\rightarrow}p$ and $p{\rightarrow}s$ are indeed the same, we find only differences in intensity but not a difference in the number of visible resonances or their frequency. The advantage of this is that a single measurement with crossed polarizers can reveal resonances that would require two measurement with parallel polarizers. However, and unfortunately enough, not all resonances found in the parallel case can be recovered in a single crossed polarizers measurement. Some resonances disappear for certain $\omega_0(k_{||})$ (see for instance Fig. 1.5(c) at $\omega_0 = 0.84$ and $k_{||} = \pm 0.22$) and others are entirely absent (compare Fig. 1.2(c) with Fig. 1.5(c) at $\omega_0 = 6.25$ and $k_{||} = \pm 0.12$). It is not clear why certain resonances are not visible in the crossed polarized configuration. Another disadvantage is that separate resonances from two parallel configurations will overlap in a crossed polarizers measurement if they are close. This becomes more evident in another close-up of the transmission spectrum.

Figure 1.6 shows the transmission spectrum data in the frequency range $0.545 - 0.585\ c/a$ (or $1505 - 1402$ nm) of the ΓM configurations with parallel $s{\rightarrow}s$ (blue), $p{\rightarrow}p$ (red), and crossed $s{\rightarrow}p$ (black) polarizations, measured at $-19°$ angle of incidence. Fano line-shape and Lorentzian line-shape fits (solid lines) are made to the data (circles). Dashed lines show Fano fits using fixed values for ω_0 and γ taken from the Lorentzian fits.

The two parallel polarization configurations in Fig. 1.6 each show a single Fano line-shape with distinct resonance frequency. The two resonances overlap in the crossed polarization and a double Lorentzian line-shape is revealed. The double Lorentzian is fitted easily using a fit function that is the (incoherent) sum of two Lorentzians as in Eq. 1.3. In fact, we find that fitting a Lorentzian or even a double Lorentzian can be easier than fitting a Fano line-shape. For a Fano fit, the background, resonance frequency and width are not necessarily independent fit parameters.

Table 1.4 shows the parameter values of the fitted Fano and Lorentz line-shapes in Fig. 1.6. We compare the frequency and width of the two peaks of the double Lorentzian fit to the values found in the two Fano fits. We find that the Lorentzian fit has smaller statistical errors, i.e. all parameters can be fit nearly $10\times$ more precise than the Fano fit parameters. It is also apparent that the frequency parameters of the Fano no longer match with the Lorentzian, the two Fano resonances are diverging from each other and from the double Lorentzian. While we find them to be degenerate near normal incidence (see Fig. 1.4), at $-19°$ the frequencies are significantly different. Comparing the widths of the resonances, we find that $\gamma \approx \gamma'$, the two resonances seem very similar. However, the values of γ, γ' of the Lorentzian are very different from those of the Fano fits. This significant difference in the resonance width is

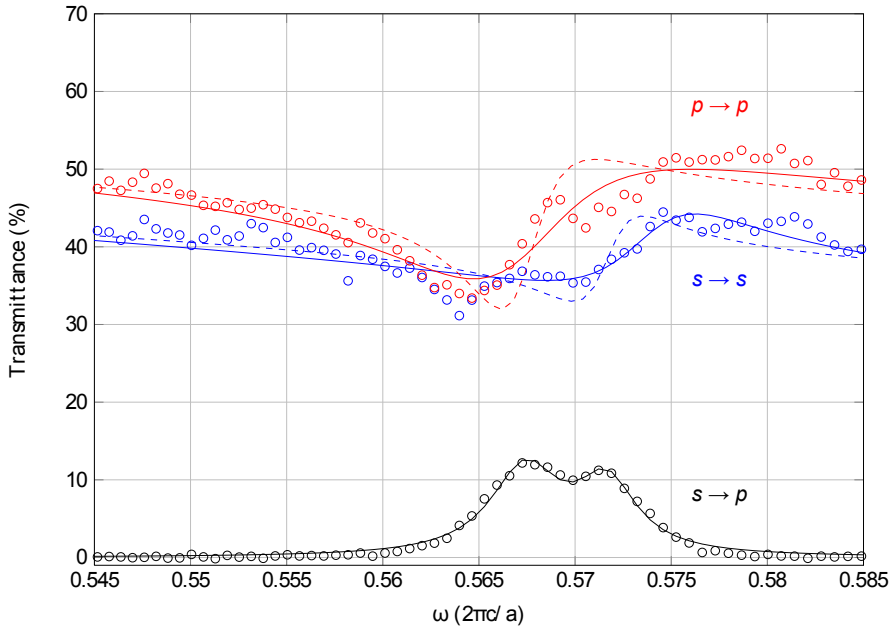

Figure 1.6: Detail of the transmission spectra of the ΓM configurations with parallel $s \rightarrow s$ (blue), $p \rightarrow p$ (red), and crossed $s \rightarrow p$ (black) polarizations, measured at $-19°$ angle of incidence. Solid lines show Fano line-shape and Lorentzian line-shape fits to the data (circles). The black data is multiplied $10\times$ for visibility. Dashed lines show Fano fits using fixed values for ω_0 and γ taken from the Lorentzian fits (see text).

immediately visible as we fit the Fano line-shapes again using dashed lines in Figure 1.6 using the ω_0 and γ parameters from the Lorentzian results. The Lorentzian resonances appear to be more than two times sharper than their Fano companions. It is not exactly clear and beyond the scope of this thesis why the double Lorentzian is not matching the two Fano line-shapes in frequency as well as in width.

	$p \rightarrow p$	$s \rightarrow p$	$s \rightarrow s$
ω_0	0.568 ± 0.001	0.5674 ± 0.0002	——
ω_0'	——	0.5716 ± 0.0001	0.574 ± 0.001
γ	0.005 ± 0.001	0.0022 ± 0.0002	——
γ'	——	0.0019 ± 0.0002	0.004 ± 0.001

Table 1.4: Fit parameters and their values (with 95% confidence bounds) for the two Fano and the double Lorentzian fits displayed in Fig. 1.6.

2.3 Slab waveguide model

In this section we will provide a simple model that can explain the observed resonances as a function of angle of incidence. To this end we will first discuss the properties of a slab waveguide without holes.

Figure 1.7 shows a schematic diagram of a slab waveguide. The slab of thickness t is a two-dimensional uniform dielectric layer with high refractive index n_2. It is sandwiched between the ambient layer with index $n_1 < n_2$ and the substrate with index $n_3 < n_2$. The light is confined to the slab via total internal reflection at top and bottom interfaces for light rays traveling inside the slab at angles below critical angle. The ray optics picture helps to understand how the light can be bound to the slab, but does not contain the phase of the light waves upon propagation and reflection at the interface.

A more complete description is obtained by solving Maxwell's equations with boundary conditions imposed by the two interfaces of the slab [6]. Electromagnetic radiation in the slab waveguide have solutions with electric field pointing parallel to the plane of the slab (TE modes) and those that have electric field components perpendicular to this plane (TM modes). The wave solutions are expected to be exponentially decaying outside the slab and are sinusoidal inside the slab. The boundary conditions require that the parallel components of the fields are continuous at the interfaces. The wave equation is solved numerically to obtain the dispersion relation for the waveguide modes. The first few TE and TM solutions are displayed in the dispersion diagram in Fig. 1.7(b).

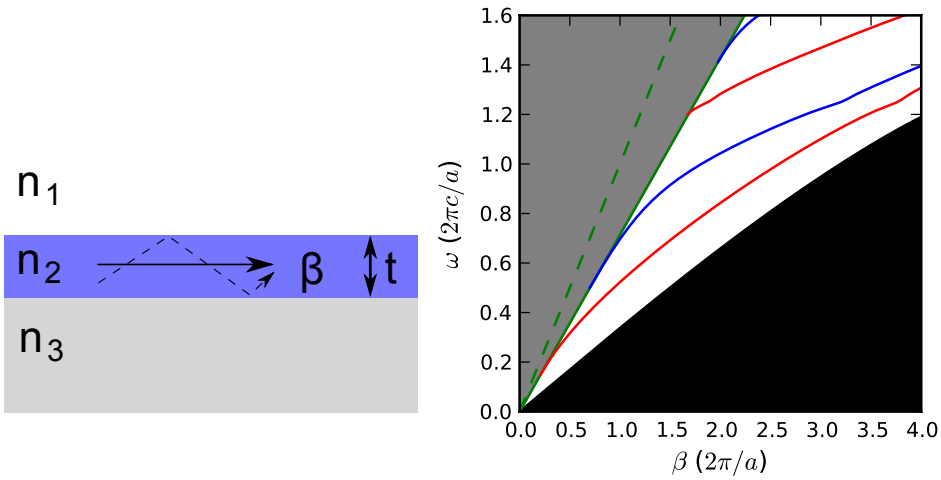

(a) (b)

Figure 1.7: (a) Schematic side view of the 2-D slab waveguide with thickness t, index $n_2 > n_1, n_3$. Total internal reflection leads to modes with propagation constant β. (b) Dispersion diagram of the slab waveguide. The red and blue lines indicate the TE and TM modes. The gray area indicates the light cone where solutions exist that propagate outside the slab. The black area does not allow any modes. The green line is the light line for n_3 (dashed for n_1).

In the slab waveguide, the modes are guided along the slab and do not couple to the radiation outside the slab. This can already be understood from the ray optics picture and also from the dispersion diagram in Fig. 1.7(b). The guided mode solutions (red and blue lines) do not cross the light cone where solutions exist that have a propagating component away from the slab (the area shown in gray), i.e. the two types of radiation are separated from each other.

The effect of a periodic lattice of holes in a slab waveguide is twofold:

(i) Modification of refractive index. Introducing holes with refractive index equal to the ambient (n_1), the average effective index of the slab n_2 is modified. As $n_1 < n_2$, the effective index will be lowered. Furthermore, the presence of holes makes n_2 dependent on the polarization of the field. For TE (TM) modes, the electric (magnetic) field will point along the slab and perpendicular to the axis of the cylindrical holes. For TM modes the electric field is parallel to the axis of the cylindrical holes. Radiation will propagate with different n_2 as the oscillating charge distribution (polarizability) is different for TE and TM modes.

(ii) Diffraction by the periodic lattice. The modulated refractive index of the slab causes the light in the waveguide to be scattered as it propagates across the holes. Since the holes form a periodic lattice, phase matched scattered light will form constructive inference, i.e. diffraction. The diffraction

allows light to escape (or enter) the slab at specific diffraction angles and the waveguide become so-called *leaky* waveguide modes. Figure. 1.8(a) shows a schematic of the diffraction process for a waveguide with a periodic lattice of holes. Diffraction thus enables the coupling of waveguide modes with external radiation. The diffraction back into the slab corresponds to the modes folded in the dispersion diagram (Fig. 1.7(b)) by adding a reciprocal lattice vector, see Fig. 1.8(b) [7, p.160], [8, p.118]. For a square lattice in a plane, the modes are translated and reflected in two dimensions, i.e. by any reciprocal vector $\vec{G} = (G_x, G_y)$. Note that Fig. 1.8(b) also includes negative β values that correspond to modes propagating in the opposite direction.

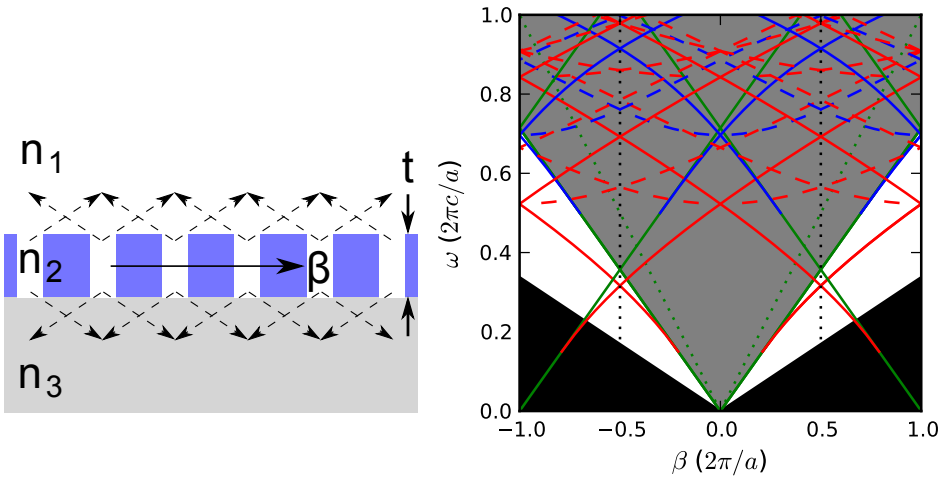

(a) (b)

Figure 1.8: (a) Schematic cross section of the waveguide slab of thickness t with a square periodic lattice of holes with a pitch a. Diffracted light indicated by dashed arrows escapes (or enters) modes in the slab indicated with propagation constant β. (b) Dispersion diagram of the slab waveguide with holes for modes propagating in the ΓX-direction, i.e. $\vec{\beta} = (\beta_x, 0)$. The first TE (red) and TM (blue) modes are folded along reciprocal vectors $\vec{G} = (G_x, G_y)$. Modes with dashed lines have $G_y \neq 0$ and illustrate the 2-D effect of the square lattice.

Comparison to experiment

In Figure 1.9 we compare the dispersion diagram of the folded waveguide modes to the dispersion diagram of the resonances found in the transmission measurements of the photonic crystal slab between parallel polarizers. This comparison is done by plotting the calculated modes on top of the transmission measurements and by manually changing the parameters of the calculation such that the modes fit best to the resonances by visual inspection. All configurations (shown in the four panels) use the same parameters

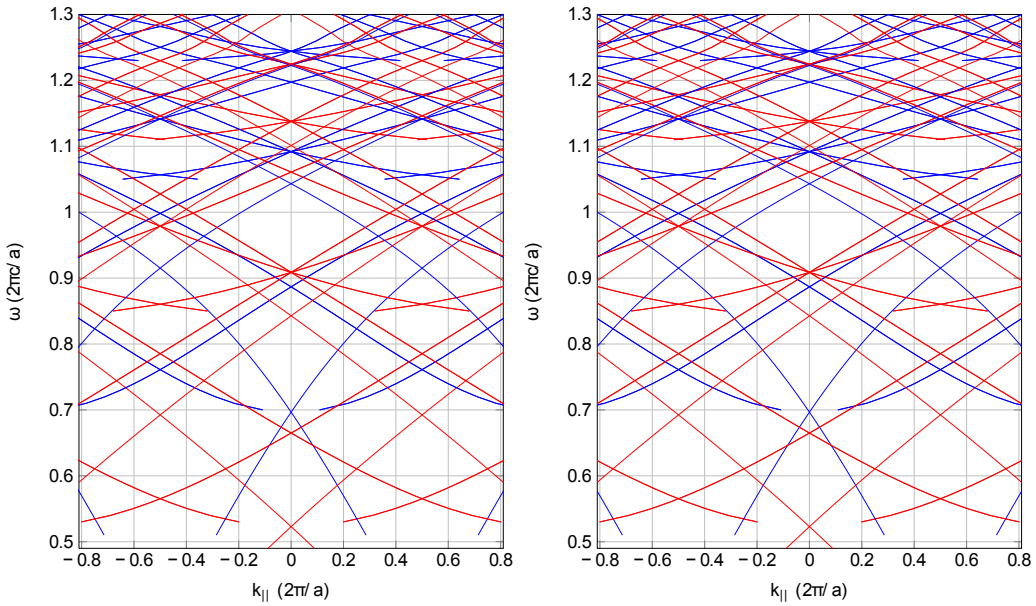

(a) ΓX $s \to s$ (b) ΓX $p \to p$

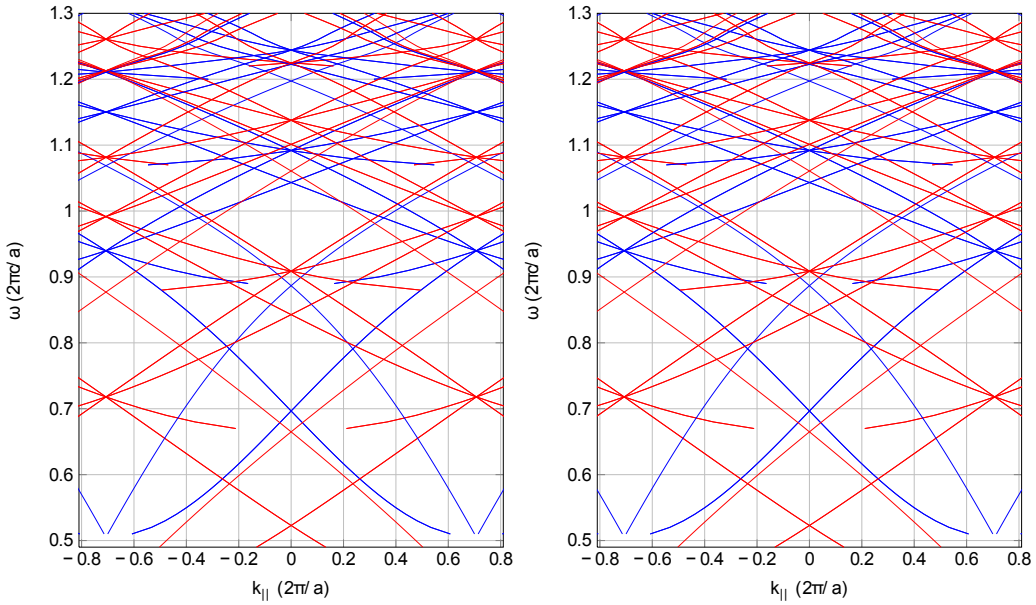

(c) ΓM $s \to s$ (d) ΓM $p \to p$

Figure 1.9: Measured transmission of a square lattice photonic crystal slab with a pitch of $a = 820$ nm. Transmission is shown as a grayscale plot as a function of in-plane wavevector $k_{||}$ (horizontal axis) and dimensionless frequency ω (vertical axis). Data is identical to Fig. 1.2. Red (blue) lines show the TE (TM) modes of the slab waveguide model fitted manually to match the visible resonances by adjusting effective dielectric constant and slab thickness (see text).

and are inspected simultaneously to judge the amount of overlap between calculation and experiment. We aim to match as many modes possible to the visible resonances, throughout the whole diagram.

	Value	Parameter Description
ϵ_1	1.0	Dielectric constant in ambient layer
ϵ_{TE}	$\epsilon(\omega) - 1.2$	Effective ϵ in guiding layer for TE solutions
ϵ_{TM}	$\epsilon(\omega) - 0.6$	Effective ϵ in guiding layer for TM solutions
ϵ_3	1.4^2	Dielectric constant in substrate
$\epsilon(\omega)$	[Fig. 1.10]	Dispersive ϵ of bulk $Al_{0.35}Ga_{0.65}As$ from [9, 10]
t	122 nm	Thickness of the guiding layer

Table 1.5: Parameters and values used for calculating waveguide modes.

Table 1.5 shows the values of the parameters used in all the waveguide calculations (presented in Fig. 1.9 and also in Figs. 1.7(b), 1.8(b)). The parameters ϵ_1 and ϵ_3 are the dielectric constants of the ambient layer (air) and substrate layer (gel) respectively, these values are known material constants and are therefore fixed. The parameters ϵ_{TE} and ϵ_{TM} are the effective dielectric constants for the photonic crystal slab for TE and TM modes respectively. Their value depends on the fill fraction of air and on the refractive index of the slab material, $Al_{0.35}Ga_{0.65}As$. The refractive index of this semiconductor is dispersive and varies strongly for photon energies ($\hbar\omega$) close to the electronic band gap energy (E_g) i.e. $\omega \approx 1.2 \cdot (2\pi c/a)$ [9, 10], for the lattice studied here. We use the measured dispersive refractive index $n = n(\omega)$ shown in Fig. 1.10 as the basis for finding an approximate effective dielectric constant of the slab. Tuning ϵ_{TE}, ϵ_{TM} will shift the calculated modes in the dispersion diagram. Also the slab thickness t is varied to match the modes with the measured resonances. Tuning ϵ and t will slide the balance between geometric dispersion (where the field distribution is mostly on the edges of slab and holes) and material dispersion (most of the field will be in the bulk material). As TE and TM modes have different field intensity distributions in the photonic crystal, ϵ_{TE} and ϵ_{TM} are separately optimized.

As can be seen in Fig. 1.9 the agreement between this simplified picture of waveguide modes and the data is very good. Further refinements, that include interaction between modes leading to avoided crossings or a complete calculation of photonic band structure are needed to improve this.

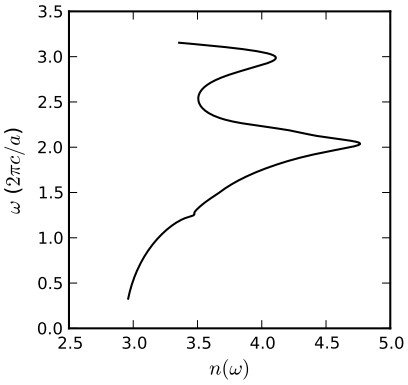

Figure 1.10: Measured refractive index of homogeneous $Al_{0.35}Ga_{0.65}As$ as a function of frequency. These values are used as $\epsilon(\omega) = n(\omega)^2/c^2$ in ϵ_{TE} and ϵ_{TM} in order to calculate the waveguide modes in Figs. 1.7, 1.8, 1.9.

3 Conclusion

We have performed linear transmission measurements in the spectral range 650 — 1700 nm on an $Al_{0.35}Ga_{0.65}As$ square slab photonic crystal with pitch $a = 820$ nm placed on a gel substrate. We varied the angle of incidences from $-50°$ to $50°$ oriented along lattice directions ΓX and ΓM and used polarizers in two parallel configurations (s and p) and two 90° crossed configurations.

The results in the case of parallel polarizers show dispersive features on top of a slowly varying background. The frequency of these features show mirror symmetry in the in-plane wave vector relative to the Brillouin zone boundaries (at $k_{||} = \pm\pi/a$) of the photonic crystal. The dispersive features found in the spectra are shown to be Fano resonances arising from the interference of a direct channel of light transmitted through the slab and an indirect, resonant, channel of light that diffracts at the crystal and propagates in the slab before it diffracts outward. The asymmetric Fano line-shape fits well to the data.

In the case of crossed polarizers, the direct channel is switched off and the background vanishes from the spectrum while the resonance feature remains visible. We recognize that the Fano line-shape is reduced to a symmetric Lorentzian line-shape. The fits show that the spectral width of the Lorentzian is significantly sharper.

The dispersion diagrams of the crossed polarized configurations $s \rightarrow p$ and $p \rightarrow s$ are found to be identical. Lorentzian line-shapes appear throughout

the dispersion diagram, most clearly for ΓM orientation, and all features correspond to resonances found in the parallel polarizers measurement although not all resonances are recovered. Fitting a Lorentzian, even a double Lorentzian, proves to be easier than fitting its Fano companion and it produces more precise values of frequency and spectral width. However, the Lorentzians are sharper and their frequencies deviate from the Fano fittings.

We introduce a slab waveguide model in order to explain the observed resonances as a function of angle of incidence. The sample has a number of guided modes bound to the slab via total internal reflection. These modes become leaky as holes are introduced that allow coupling with the external radiation via diffraction at the periodic lattice. The guided modes are calculated from Maxwell's equations with boundary conditions at the two air-slab-gel interfaces and yield TE and TM modes. The modes in the dispersion diagram are then folded by adding reciprocal lattice vectors, effectively treating the holes as a weak perturbation.

The leaky waveguide mode solutions are visually compared to the experiment by over-plotting them on the measured dispersion diagram. By tuning the slab thickness and the effective dielectric constants for TE and TM solutions (separately), we shift the calculated modes to match the visible resonances. The effective dielectric constant is dispersive and based on that of homogeneous $Al_{0.35}Ga_{0.65}As$. We find good agreement between measured resonances and calculated modes.

Part 2

Second Harmonic Generation

1 Experiment

The second harmonic (SH) generation experiments described here are performed using the setup depicted in Fig. 2.1. The pump light source is a Cobolt Tango semiconductor 5 KHz pulsed laser (PL) operating at $\lambda_p = 1535$ nm. The light is attenuated to the desired power and linearly polarized by means of two Glan-Thomson polarizing beam splitters (Pol_1 and Pol_2). Another such polarizer at the detector end is used as an analyzer. We set polarizer and analyzer individually to s or p*, thus providing parallel ($s \rightarrow s$, $p \rightarrow p$) and crossed ($s \rightarrow p$, $p \rightarrow s$) polarization configurations. In order to measure the generated SH light intensity, the photonic crystal sample is imaged onto a CCD camera (512px×768px Apogee Alta U1) using a single lens. The incident light is filtered using a long pass filter at 1400 nm. The detected light is filtered using a short pass filter at 800 nm and a narrow band pass filter at 766 nm. These color filters (and proper shielding) are to ensure that only the SH signal from the sample is detected. A power meter (PM) is used to check laser power before performing measurements. A narrow band mirror at 766 nm on a flip-stage enables measurement of SH light in reflection as well as in transmission.

We perform the experiments on a photonic crystal slab of $\text{Al}_{0.35}\text{Ga}_{0.65}\text{As}$ with a square lattice of holes with radius of ~ 150 nm and lattice constant or pitch $a = 820$ nm. The lattice of holes is fabricated using e-beam lithography and reactive ion etching techniques. The slab thickness is ~ 150 nm and of size $\sim 300 \times 300$ μm^2. The photonic crystal is placed on a transparent gel substrate with index $n_{\text{gel}} = 1.4$ which in turn sticks to a glass microscope

*Where s (senkrecht) and p denote the polarizations perpendicular to and parallel to the plane of refraction, respectively.

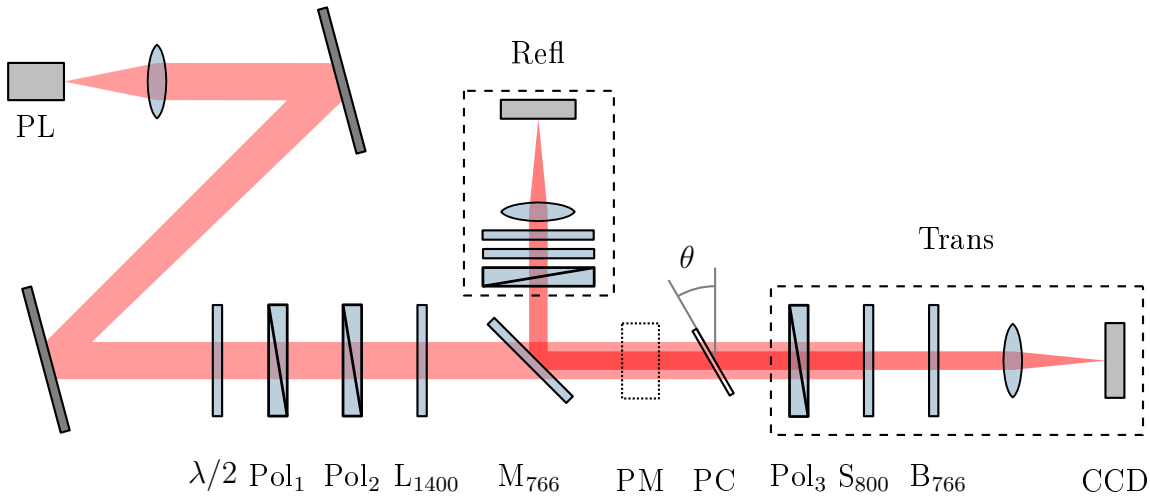

Figure 2.1: Experimental setup to detect second harmonic with a CCD camera generated in the photonic crystal sample (PC). PL indicates the pulsed laser source generating the collimated laser beam at $\lambda_p = 1535$ mm. The beam is attenuated using two polarizing beam splitters Pol_1 and Pol_2. L_1400 indicates a 1400 nm long-pass filter. A narrow band mirror at 766 nm (M_{766}) on a flip-stage allows reflection measurements (the Refl path is identical to the Trans path). Optionally, a power meter (PM) is inserted. The generated light from the PC is filtered with a polarizer (Pol_3), a 800 nm short-pass filter (S_{800}) and a narrow band-pass filter (B_{766}).

slide [1]. In this asymmetric sample we have chosen to perform most (transmission) measurements with the orientation such that the light propagates in the direction gel-pc-air. The microscope slide is cut and attached to a ring mount which allows manual alignment of the orientation of the photonic crystal axis relative to the vertical rotation axis. We orient the sample so that the parallel component of the wavevector of the incident light is either along the ΓX or ΓM symmetry directions of the photonic lattice. To align the parallel component of the wavevector along the symmetry directions, we identify the orientation of the diffraction spot pattern of the lattice formed by the laser beam on a piece of millimeter paper. Two horizontal translation stages allow centering of he sample mount to the rotation axis. A motorized rotation stage allows automation of transmission experiments with varying angle of incidence. The ring mount is made thin to allow for transmission measurements at oblique angles up to ±50° from normal incidence. Two more horizontal translation stages allow alignment of the rotation axis to intersect with the optical axis and focal point. A vertical translation stage allows alignment of the sample to the focal point.

Table 2.1 lists the configurations for which we have measured the second harmonic generation in the photonic crystal (PC) sample. For conciseness, not all measurements listed here are presented as a graph in this report. To get sufficiantly high signal-to-noise ratio, we varied the integration time necessary to collect the SH signal greatly as a function of the angle of incidence. The integration time is set by trial and error and ranges from 10 s to 1 h. The reference signal is a dark measurement with the laser light blocked and is measured automatically in every configuration and for most angles of incidence. To save time, dark measurements are skipped for some angles of incidence (in case of small angle steps).

Sample orientation	Transmission	Reflection
ΓM gel-pc-air	s, p, $s \to p$, $p \to s$	p
ΓM air-pc-gel	s, p	p
ΓX gel-pc-air	p	—
ΓX air-pc-gel	—	—

Table 2.1: Overview of the selected configurations for which second harmonic generation in the photonic crystal slab (pc) is measured (as a function of angle of incidence).

1.1 CCD intensity measurement procedure

The setup uses a CCD camera to measure the intensity of the SH generated light. The individual pixels of the CCD camera are highly sensitive and have a relatively low dark current due to their small size. By illuminating multiple pixels, the dynamic range can be extended well beyond the dynamic range of an individual pixel. An additional advantage of employing the CCD camera is the large collection area of the CCD which makes alignment easy and removes the requirement to realign in order to optimize the signal every time the sample is rotated.

In order to obtain a single, accurate value of the overall intensity of the SH signal the camera images must be analyzed and corrections must be made before pixel values are summed. The procedure is described below.

1. A recorded CCD image is saved as raw binary data file (512×768 uint16 array) for every angle of the measurement run. This uncompressed, lossless file format is fast, it can be directly written by LabVIEW and it loads directly into Matlab as a 2D array.

2. A region of interest (ROI) is determined for the whole run of the measurement by manual visual inspection of all images. The ROI size is chosen to be *just* large enough to capture the largest spot size in the run and allowing a wobble (in position and shape) of the spot as the sample is rotated. The same ROI is used on dark measurement images. In this way the amount of dark counts is minimized without discarding signal. This thus comprises a stable algorithm to maximize signal-to-noise.

3. Another ROI (noise ROI) is determined for the purpose of collecting the background noise of each image. The noise ROI is a region away from the spot ROI. Again, dark images have the same noise ROI collected.

4. So-called hot pixels are pixels on the CCD that are permanently energized and show up as pixels with high intensity (values over 12000/65535) which increase error in the intensity measurement. These hot pixels become apparent at long integration times. The hot pixels are automatically identified in the dark image as having a value larger than a manually determined threshold value. To exclude hot pixels, they are overwritten with zeros in both light and dark measurement images.

5. The total intensity of the SH spot is calculated. The spot signal is calculated by subtracting the dark image ROI from the light image ROI and taking the sum. Not all light images with angles α (ImgL(α)) have dark images, so the dark image with nearest angle α' (ImgD(α'))

is used. The intensity sum is normalized by the integration time T. Also the intensity sum of the noise ROI is calculated this way.

$$I_{\mathrm{ROI}}(\alpha) = \frac{1}{T} \sum_{\mathrm{ROI}} [\mathrm{ImgL}(\alpha)(x,y) - \mathrm{ImgD}(\alpha')(x,y)]$$

6. The SH signal result (as plotted in the following sections) is calculated by taking the absolute difference of the spot intensity (to avoid negative numbers) and noise intensity to remove the noise floor from the signal.

$$I(\alpha) = \left| I_{\mathrm{spot}}(\alpha) - I_{\mathrm{noise}}(\alpha) \right|$$

Figure 2.2 shows an example CCD intensity measurement image removing hot pixels and normalizing to T (i.e. after step 5. of the protocol). It is captured at angle of incidence $\alpha = -34.25°$ (corresponding to $k_{||} \approx -0.30$ at $\lambda_{\mathrm{pump}} = 1532.9$ nm) in configuration ΓM, s-pol, gel-pc-air. The full region of interest is shown, indicating that the maximum extent of the spot (found near normal incidence) is larger than the spot visible here. This angle corresponds to the minimum value of SH signal. This indicates that the SH value shown at this angle is well above the noise.

2 Results

First we present linear transmission measurements at the fundamental (pump) frequency as well as linear measurements at double the fundamental frequency (second harmonic frequency).

2.1 Linear measurements

Figure 2.3 displays a selection of the linear transmission spectroscopy measurements performed on the photonic crystal sample, as described in Part 1. The selected region is near the laser pump frequency $\omega_p = 0.53507$ ($=a/\lambda_p = 820/1535$) that is used in the second harmonic generation measurements. The transmission spectrum shows the dispersive Fano-lineshape feature that has a fitted resonance frequency of $\omega = 0.53450$ at normal incidence, thus coinciding with laser pump.

Figure 2.4 shows the linear transmission spectra in the region near the second harmonic frequency $2\omega_p = 1.0690$ of the photonic crystal sample in between parallel polarizers ($s \to s$) and crossed polarizers ($p \to s$), for angles of incidence from normal incidence $-8°$ to $+8°$ in $0.25°$ steps.

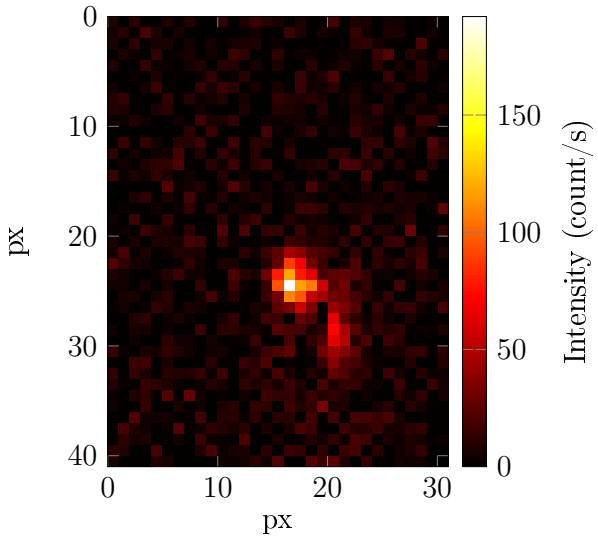

Figure 2.2: Example CCD intensity measurement image (hot pixels removed, intensity normalized to integration time) captured at angle of incidence $\alpha = -34.25°$ (corresponding to $k_{||} \approx -0.30$ $(2\pi/a)$ at $\lambda_{\text{pump}} = 1532.9$ nm) in configuration ΓM, s-pol, gel-pc-air (see Fig. 2.6(a)). The full region of interest is shown, indicating that the maximum extent of the spot (found near normal incidence) is larger than visible here.

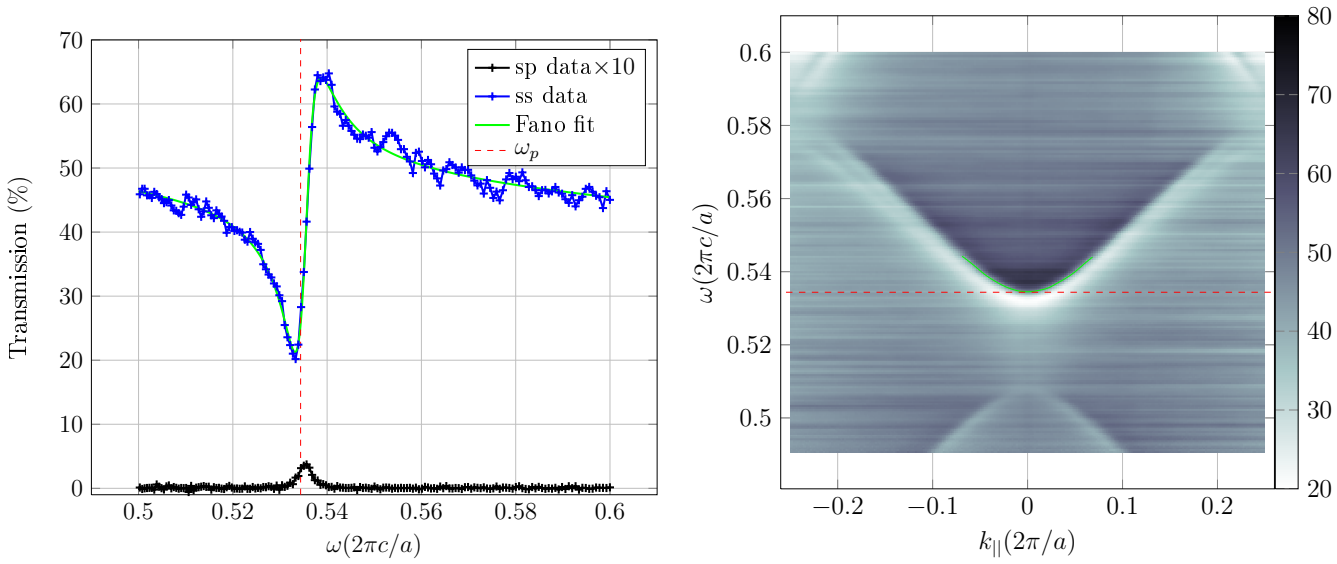

(a) (b)

Figure 2.3: Linear measurements of the photonic crystal sample (in ΓM orientation) showing the region nearby the laser pump frequency $\omega_p = 0.53507$ ($\lambda_p = 1535$ nm), indicated with the red dotted line. (a) Shows transmission spectra near normal incidence of the sample in between parallel polarizers ($s \rightarrow s$ in blue) and crossed polarizers ($s \rightarrow p$ in black). The data is identical to data represented in Fig. 1.4. The Fano lineshape is fitted to the observed resonance (shown in green). (b) Shows the dispersion diagram of the parallel tranmission measurements. Fano fits are performed to spectra of off-normal angles as well and the obtained resonance frequency as a function of $k_{||}$ is plotted in green.

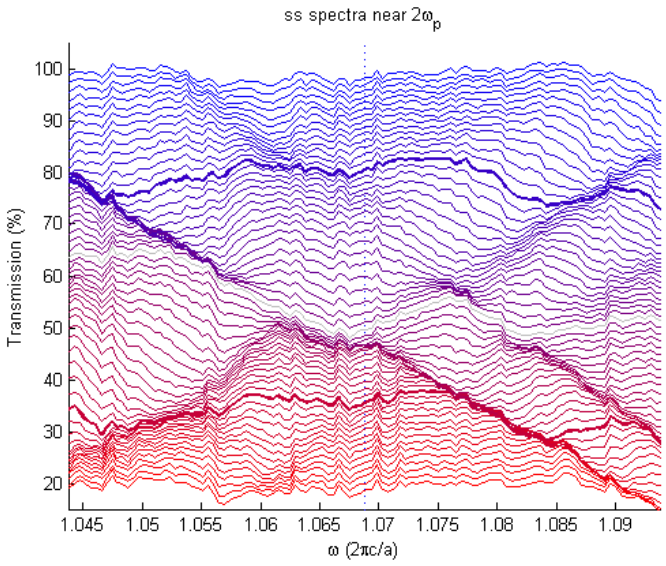

(a)

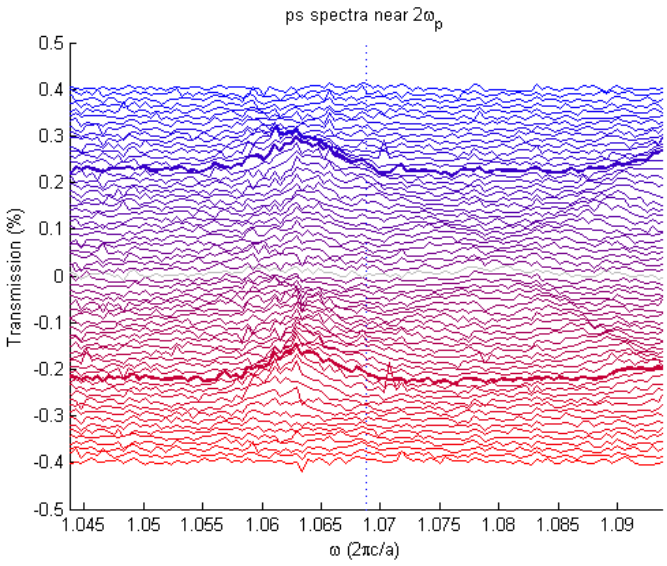

(b)

Figure 2.4: Linear transmission spectra in the region near the second harmonic frequency $2\omega_p = 1.0690$ of the photonic crystal sample (ΓM orientation along $k_{||}$) in between parallel polarizers ($s \to s$) and crossed polarizers ($p \to s$), for angles of incidence from normal incidence $-8°$ to $+8°$ in $0.25°$ steps. Three spectra are highlighted with thick lines. One is normal incidence (in gray) and the other two correspond to the angle of the "side lobes". The second harmonic frequency is indicated with a dotted line.

2.2 Nonlinear measurements

Power measurement

A prerequisite measurement to the second harmonic experiment is a power measurement in order to confirm the nonlinearity of the signal power as a function of input power. The pump power is measured by inserting the power meter (PM) in front of the photonic crystal, as shown in the setup in Fig. 2.1. In Figure 2.5 the intensity of the second harmonic signal is plotted on a log-log scale as a function of input pump power. A linear fit to the data yields a slope of 1.94 ± 0.44. This confirms the expected squared power dependence of the SH signal.

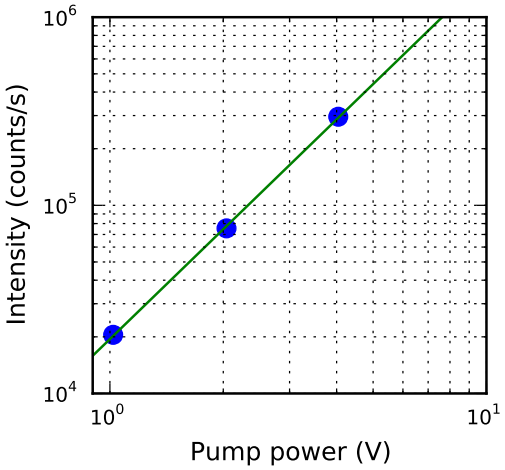

Figure 2.5: Measurement of the second harmonic signal vs input pump power. Blue dots indicate data. The green line shows a linear fit (on the log-log scale) to the data and has a slope of 1.94 ± 0.44.

SHG intensity vs angle of incidence

Figure 2.6 Displays the measured second harmonic response of a square lattice photonic crystal slab with a pitch of $a = 820$ nm illuminated by a pump laser beam operating at $\lambda_p = 1535$ nm. The setup is set in transmission configuration, with the slab in gel-pc-air orientation. The crystal is aligned such that crystal axis ΓM points along wavevector $k_{||}$, which is the component of the incident wavevector along the surface, i.e. $k_{||} = k \sin\theta = \frac{\omega}{c} \sin\theta$, where θ is the angle of incidence. The photonic crystal sample is sandwiched between parallel polarizers in s-polarizaton (a) or in p-polarization (b). The intensity of the SH signal is plotted logarithmically as a function of $k_{||}$.

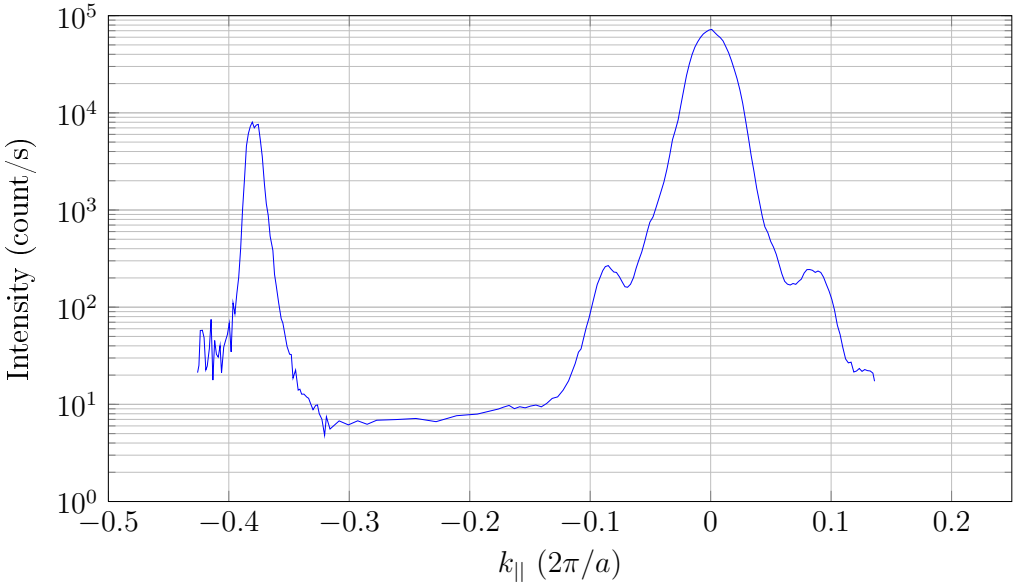

(a) s-polarization

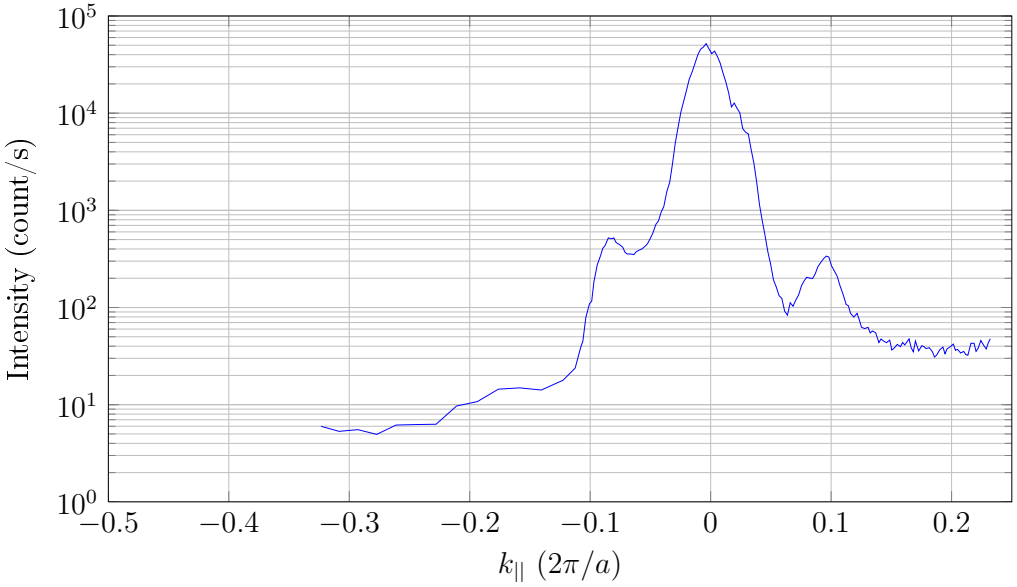

(b) p-polarization

Figure 2.6: Second harmonic generation measurements of a photonic crystal slab with a pitch of $a = 802$ nm, illuminated by a $\lambda_p = 1535$ nm pump laser. The setup is in transmission configuration, with the slab in gel-pc-air orientation and the crystal axis ΓM along in-plane wave vector $k_{||}$. The sample is sandwiched between polarisers in s-polarization (a) or in p-polarization (b). The SH signal intensity is plotted on log scale as a function of $k_{||}$.

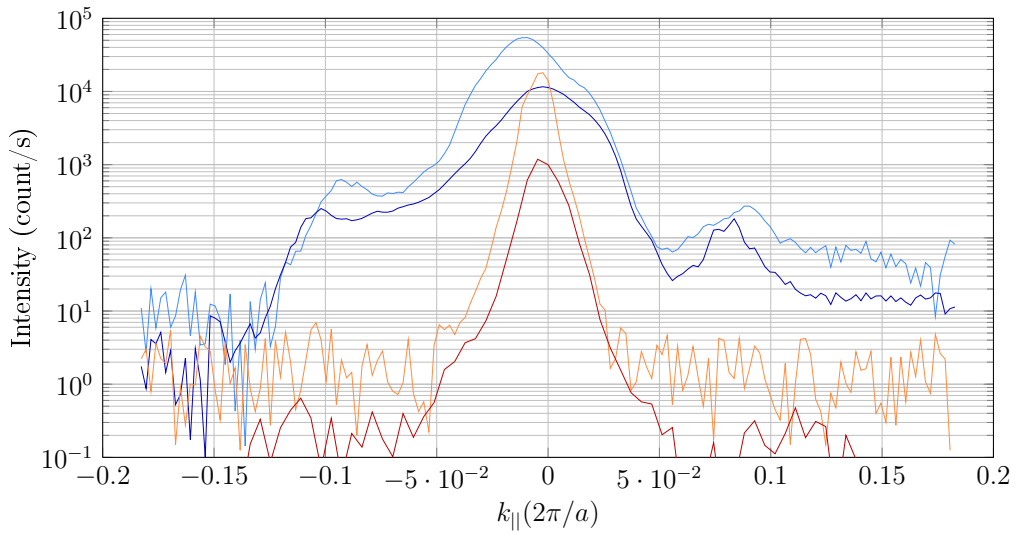

Figure 2.7: Second harmonic generation measurements of a photonic crystal slab with a pitch of $a = 802$ nm, illuminated by a $\lambda_p = 1535$ nm pump laser, sandwiched between p-polarizers. In-plane wave vector $k_{||}$ points along crystal axis ΓM. Blue curves indicate Transmission measurements (7 s and 40 s), red curves indicate Reflection measurements (40 s and 500 s), and light (dark) tinted curves incidate gel-pc-air (air-pc-gel) illumination direction.

The second harmonic generated intensity range spans over four decades depending on the angle of incidence. In order to collect this range, different measurement runs with integration times ranging from 10 seconds to 1 hour have been used to compile this figure. The noise floor is different for every integration time and fluctuations in the result indicate a lower signal to noise. The maximum intensity $I > 7.2 \cdot 10^4$ count/s ($> 5.19 \cdot 10^4$ for p-polarization) is found at normal incidence and a second local maximum ($> 8 \cdot 10^3$ count/s is found at $k_{||} = 0.38$, corresponding to an angle of incidence $\arcsin(-0.38 \cdot 1535/820) = -45.25°$. Symmetric about normal incidence we find two local maxima of intensities 268 count/s and 243 count/s at $k_{||} = -0.085$ and $k_{||} = 0.082$, respectively. We call these local maxima "side-lobes." The overall minimum with intensity $I \approx 5$ count/s is found near $k_{||} = -0.31$ (corresponding to $\alpha = -35.41°$)

Configuration dependence of SHG signal

Figure 2.7 shows the results for four measurements of the second harmonic signal around normal incidence. We compare the second harmonic intensity signal generated in the photonic crystal (pc) slab in case of illumination of

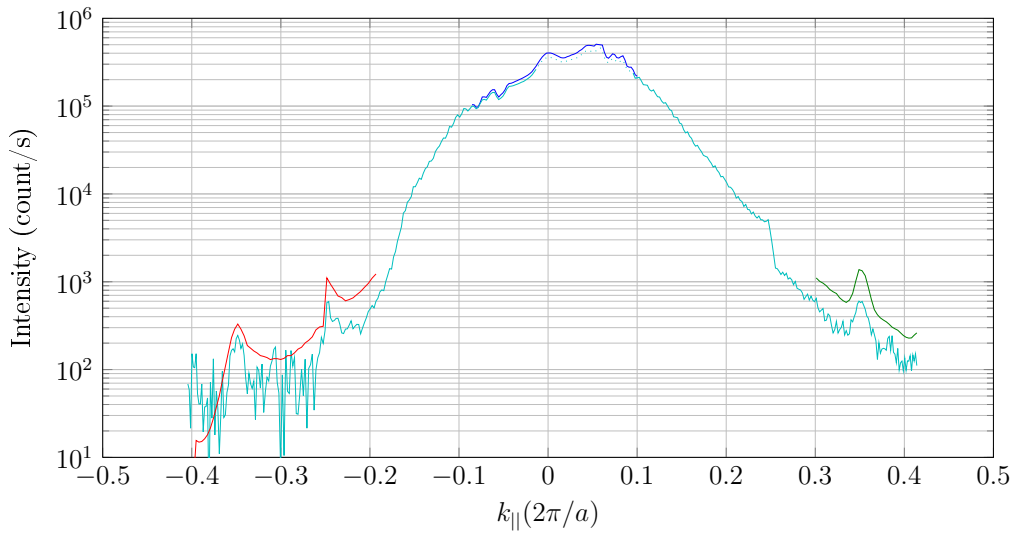

Figure 2.8: Second harmonic generation measurements of a photonic crystal slab with a pitch of $a = 802$ nm, illuminated in gel-pc-air direction by a $\lambda_p = 1535$ nm pump laser. In this alignment, crystal axis ΓX is parallel to in-plane wave vector $k_{||}$. The sample is sandwiched between p-polarisers. Different data series with integration times (1 s, 2 s, 400 s and 400 s) are indicated with different colors (blue, cyan, red and green, respectively).

the pc in gel-pc-air order with illumination in air-pc-gel order. We compare also the measured SH signal in case of detection using the Transmission setup configuration with detection using the Reflection setup configurations.

Note that all p-polarized measurements shown in Fig. 2.7 are not symmetric about normal incidence. The intensity is not only higher when the SH signal is measured in Transmission configuration, the shape of the central peak is also narrower. Overall, it is apparent that the illumination of the crystal slab in gel-pc-air direction generates a (as much as 10×) brighter SH spot.

Figure 2.8 shows second harmonic generation measurements of the photonic crystal slab where the crystal axis ΓX is aligned parallel to in-plane wave vector $k_{||}$. The sample is the same with a pitch of $a = 802$ nm and is illuminated in gel-pc-air orientation by the $\lambda_p = 1535$ nm pump laser. The sample is sandwiched between p-polarisers. This figure shows different measurement series with integration times (1 s, 2 s, 400 s and 400 s), which are indicated with different colors (blue, cyan, red and green, respectively).

Note that the different measurements in Fig. 2.8 are chosen such that the first measurement has its underexposed (overexposed) parts replaced with the red and green (blue) measurements. The overall shape of the intensity

curve is clearly less peaked compared to the the ΓM measurements above.

3 Discussion

The second harmonic generation experiments on photonic crystal slab presented here demonstrate that second harmonic generation can be significantly enhanced by the photonic lattice. We compare the minimal SH signal (~ 5 count/s) with the maximum SH signal ($> 7.2 \cdot 10^4$ count/s)[†] in Fig. 2.6(a), and we find an enhancement $> 10^4$.

We present a simple model that describes the dependence of the second harmonic intensity on the parallel wavevector $k_{||}$. Second harmonic generation can be enhanced by resonances in the photonic crystal. When incident light couples to a resonance with a quality factor Q, the field amplitude at the fundamental frequency is multiplied by Q, and the second harmonic generated light is enhanced by a factor Q^2. In this simple description, the presence of resonances near the double frequency are not taken into account. The intensity of the second harmonic generation for a slap of the same thickness and effective dielectric constant as the photonic crystal structure is assumed to be found when measuring the minimum SH signal, when the pump frequency is not near any resonance mode. We neglect the possibility that the crystal structure could in fact lower the SH intensity by destructive interference effects.

The linear results (presented in Part 1 of this thesis) show the resonances for incident light that couples to the crystal modes of the photonic crystal. The laser light pumped inside the resonance has an intensity that can be described by a Lorentzian function, Equation 2.1:

$$I_\omega = \frac{I_0}{1 + \left(\frac{\omega_0(k_{||}) - \omega_p}{\gamma_{k_{||}}}\right)^2} \tag{2.1}$$

The second harmonic generated light has an intensity proportional to the square of the fundamental, resulting in Eq. 2.2:

$$I_{2\omega} \propto I_\omega^2 \tag{2.2}$$

In Figure 2.9 we fit the squared Lorentzian function (in red) to the second harmonic measurement data (in blue) from Fig. 2.6. We set $\omega_o(k_{||})$ equal to a spline function fitted to the dispersion of the fundamental resonance

[†]This is the maximum SH signal for s-polarization, for p-polarization we find $5.2 \cdot 10^4$ count/s, see Fig. 2.6(b))

frequency. The values are obtained from fitting the linear transmission results using the Fano model (see Fig. 2.3). The dispersion $\omega_0(k_{||})$ is relative to the laser pump frequency $\omega_p = 534.38$ nm. Having set the frequency, the fit parameters of the (squared) Lorentzian $I_{2\omega}(k_{||})$ are the intensity I_0^2 and the width $\gamma_{k_{||}}$. Only the data points near normal incidence are selected (indicated in black). We exclude the so-called "side-lobes" from the fit as they are clearly not represented in the shape of the Lorentzian curve. Disregarding this, we find that the squared Lorentzian function fits the peak well, both in a logarithmic plot (Fig. 2.9(a)) and in a linear plot (Fig. 2.9(b)). The squared Lorentzian fitting yields an intensity $I_0^2 = (6.805 \pm 0.119) \cdot 10^4$ and a width $\gamma_{k_{||}} = (0.00137 \pm 0.00004)$.

We highlight that the width $\gamma_{k_{||}}$ is expressed in terms of the parallel wavevector component. Therefore, it cannot be compared directly to the width γ from the frequency dependent measurements in Sec. 2.1. A conversion is between these numbers is possible, but is outside the scope of this thesis.

In Figure 2.9 we use the resonance frequency as a function of $k_{||}$ from fitting the Fano line shape to the linear spectral data. It should also be possible to obtain it via fitting the Lorentzian line shape when using crossed-polarizers. In order to use it in the squared Lorentzian fit to the second harmonic data, the dispersion of the resonance, i.e. $\omega_0(k_{||})$, has been taken into account. The width of the resonance however, which influences the coupling strength, has been left out of consideration. Work has been done to investigate this relation further, but is outside the scope of this thesis. [11]

Close to normal incidence (where the frequency mismatch is minimal) we have fitted the Fano line shape in Part 1, resulting in a quality factor $Q = \gamma/\omega_0 = 0.0027/0.5356 = 198$ (see Tbl. 1.2). From crossed-polarized spectra we have fitted the Lorentzian line shape, resulting in $Q = 0.0016/0.5356 = 335$ (see Tbl. 1.3). In the simple model, the second harmonic signal has a gain of $10^4 = Q^2$, yielding a value of $Q = 100$. This value is about half of the lowest value estimated from the Fano line-shape and $3\times$ lower than the value from the crossed polarized signal. This discrepancy might be explained by losses due to weak coupling into the crystal, possibly due to polarization effects or by the laser frequency being not exactly resonant at normal incidence. A laser detuning $\omega_p - \omega_0$ could be sufficient to explain the data.

It is clear however, that the fit does not fully describe the second harmonic results. From these figures we can identify the following features that are missing in the squared Lorentzian model, in order of size:

1. The "side-lobes" at $k_{||} \approx \pm 0.087$,

2. the tip of the peak a normal incidence, and

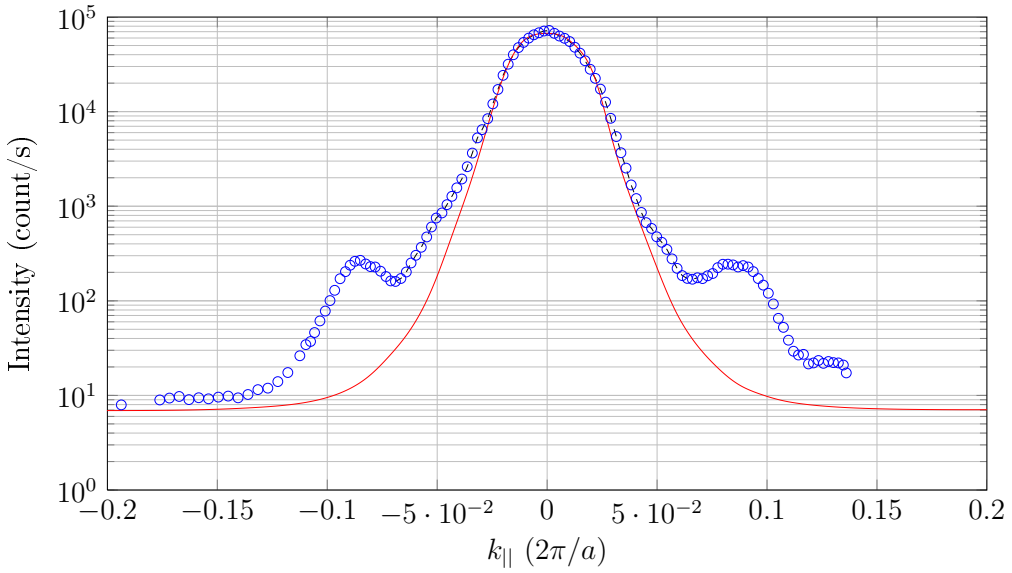

(a)

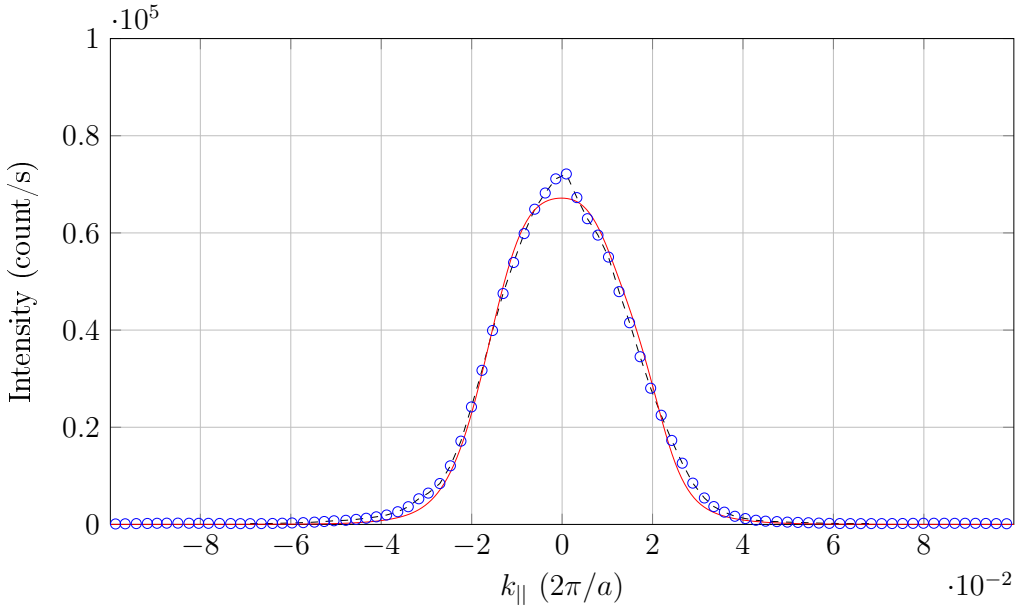

(b)

Figure 2.9: Squared Lorentzian fit (in red) on SH measurement data near normal incidence (in blue, the measurement is that of Fig. 2.6). The black dashed line indicates the range of data included in the fit. The result is plotted on a logarithmic scale in (a) and linear scale in (b).

3. the less-pronounced "side-lobes" at $k_{||} \approx \pm 0.05$.

The origin of the "side-lobes" might be found in analyzing the modes near the second harmonic frequency 2ω. We can inspect the transmission spectra of the photonic crystal in between parallel polarizers (see Fig. 2.4(b)), but it is immediately clear that the number of modes in this frequency range is high. This makes it difficult to identify which modes enhance the SH signal and even more difficult to quantify the enhancement. In the crossed-polarized spectra however, displayed in Figure 2.4(b), we can identify two resonance features near the intersection of 2ω in the spectrum at the angle of incidence corresponding to the "side-lobes." Attempts to analyze the spectra further to describe the second harmonic results have been made but are outside the scope of this thesis. [11]

4 Conclusion

We have performed second harmonic generation (SHG) measurements on a square photonic crystal made in $Al_{0.35}Ga_{0.65}As$ with a pitch $a = 820$ nm placed on a gel substrate with a pump laser with frequency $\lambda_p = 1535$ nm. We measured transmission and reflection spectra as a function of the angle of incidences up to $\pm 50°$. Measurements were done with $k_{||}$ aligned along lattice directions ΓX and ΓM. Polarizers in the beam allow to measure in a parallel configurations (s and p) and in two 90° crossed configurations ($s \to p$ and $p \to s$). A CCD camera is used to detect the second harmonic signal, employing post-processing of the image data to remove hot-pixels.

Before measuring the SH signal, we have taken linear transmission spectrum measurements near the pump frequency and the SH frequency. The photonic crystal sample has a resonant mode at normal incidence at a frequency very near the pump frequency. This allows strong coupling into the mode. At the SH frequency, we find many resonant modes that may be relevant.

The first SHG measurement is a power measurement in order to confirm that the signal has squared power dependence, as expected from SHG.

In the main SHG measurements we have measured intensity as a function of angle of incidence. Since the intensity varies orders of magnitude, different measurements with various integration times (1 s − 1 h per data point) have been patched together. Not all possible configurations of the setup have been used, most measurements were done in transmission setup with the ΓM crystal axis oriented along $k_{||}$ and having the gel substrate of the photonic crystal slab facing the incident light (gel-pc-air orientation). For this configuration,

all polarizations ($s, p \rightarrow s, p$) have been measured, at least around normal incidence.

The results show a clear maximum near normal incidence, for all measurement configurations. We calculate the gain of the SHG as the ratio of maximum intensity to minimum intensity and obtain a gain of 10^4. This enhancement in the SHG is due to the presence of a lattice of holes in the material. In a simple model, we link the overlap and quality factor of the fundamental resonance found in linear transmission spectra to the generation of light at the double frequency. The SHG gain is high, but still lower than expected ($Q^2 \sim 4 \cdot 10^4$) from the quality factor of the fundamental resonance near normal incidence ($Q \sim 200$).

We are able to fit a squared Lorentzian curve to the peak of the SH signal. This fits well, apart from two very apparent local maxima called "side-lobes" that are found at angles of incidence symmetric about normal incidence in the case of ΓM orientation with s-polarizers (they are found asymmetric for p-polarization and not apparent in ΓX). The origin of these side-lobes is expected to be found in the effect of many resonance modes of the photonic crystal present near the double frequency. Using crossed polarized linear transmission spectrum data, we are able to identify a crossing of modes near (but not spot-on) the intersection of the double frequency and the angle of incidence of the side-lobes.

Bibliography

[1] Lj. Babić, R. Leijssen, E. F. C. Driessen, and M. J. A. de Dood, "Transfer of photonic crystal membranes to a transparent gel substrate", Opt. Express 19, 19532–19541 (2011).

[2] J.D. Joannopoulos, S.G. Johnson, J.N. Winn, R.D. Meade, "Photonic Crystals: Molding the Flow of Light", 2nd Ed. (2007).

[3] U. Fano, "Sullo spettro di assorbimento dei gas nobili presso il limite dello spettro d'arco," Nuovo Cimento, N. S.,

[4] U. Fano, "Effects of configuration interaction on intensities and phase shifts." Phys. Rev. 124, 1866–1878 (1961).

[5] B. Luk'yanchuk, N.I. Zheludev, S.A. Maier, N.J. Halas, P. Nordlander, H. Giessen, and C.T. Chong, "The Fano resonance in plasmonic nanostructures and metamaterials," Nature Materials 9, 707–715 (2010).

[6] P. Yeh, "Optical Waves in Layered Media," John Wiley & Sons, Hoboken, N.J. (1998).

[7] N.W. Ashcroft, N.D. Mermin, "Solid State Physics," Harcourt (1976).

[8] J.R. Hook, H.E. Hall, "Solid State Physics," John Wiley & Sons, West Sussex, 2nd Ed. (1991).

[9] S. Adachi, "GaAs, AlAs, and $Al_xGa_{1-x}As$@B: Material parameters for use in research and device applications," J. Appl. Phys. 58, R1 (1985).

[10] S. Adachi, "Optical dispersion relations for GaP, GaAs, GaSb, InP, InAs, InSb, $Al_xGa_{1-x}As$, and $In_{1-x}Ga_xAs_yP_{1-y}$," J. Appl. Phys. 66, 6030 (1989).

[11] Lj. Babić, L.T.H. van Dellen, and M.J.A. de Dood, "Fano interpretation of second harmonic generation in a photonic crystal on a gel," Appl. Phys. Lett. 101, 261120 (2012).

Fano interpretation of second harmonic generation in a photonic crystal on a gel

Ljubiša Babić,[a] Louwrens T. H. van Dellen, and Michiel J. A. de Dood[b]
Huygens Laboratory, P.O. Box 9504, 2300 RA Leiden, The Netherlands

(Received 26 July 2012; accepted 13 December 2012; published online 28 December 2012)

We observe a 10^4 times enhancement of the second harmonic generation of 1.535 μm laser light in a two-dimensional AlGaAs photonic crystal at normal incidence. The linear properties of the optical modes that are resonant with the fundamental frequency are well described by a Fano model and have a typical quality factor of 100. We present an extended version of the Fano interpretation to quantitatively analyze the second harmonic signal using the measured linear properties as input and find good agreement with the data. © *2012 American Institute of Physics*. [http://dx.doi.org/10.1063/1.4773513]

Strong enhancement of local fields can be achieved in photonic crystals with a large refractive index contrast. This leads to a greatly enhanced light-matter interaction and provides access to non-linear optical phenomena. Of particular interest are the non-linear processes of second harmonic (SH) generation,[1–9] difference frequency generation,[10] and parametric down-conversion as they may provide on-chip nanophotonic light sources operating at frequencies that are otherwise difficult to achieve. The process of parametric down-conversion in a photonic crystal may create sources of entangled photons that are brighter than conventional sources or show dispersion characteristics that can be tuned through the design of the structure.[11–13] For efficient down-conversion, phase-matching or double resonance is essential. Unlike harmonic generation in cavities, the down-conversion process is only linearly dependent on pump power and does not benefit from strong local-field enhancements.

Leaky modes of a photonic crystal slab seem to be particularly attractive, because they combine good field confinement with a reasonable interaction length to make the interaction efficient by phase-matching the waves at the fundamental and the SH frequency. Second harmonic[1–7] and difference frequency generations[10] have been demonstrated in planar photonic crystal structures consisting of III-V semiconductor materials that have large second-order non-linearities. So far, experiments investigated the non-linear processes in reflection and at oblique angles of incidence using ultrashort femtosecond laser pulses. These studies report a 1000 times enhancement in SH generation1 for a two-dimensional structure.

In this letter, we demonstrate resonant SH generation at normal incidence in the transmission of a two-dimensional photonic crystal transferred to a gel.[14] In contrast to earlier work, we use a narrow linewidth pulsed laser to ensure that the laser is fully resonant with the structure and measure a 10^4 times enhancement. We extend a Fano model that describes the linear optical properties of the photonic crystal[15,16] to describe SH generation using the measured quality factors and frequencies as input. This is an advantage over purely numerical finite difference time domain or Green's function[17] methods. These methods tend to overestimate quality factors and enhancement factors by assuming ideal structures in order to limit computational resources.

The photonic crystals have a lateral size of $300 \times 300\ \mu m^2$ and consist of a square lattice of ~150 nm radius holes with a lattice constant $a = 820$ nm ($r/a = 0.18$) patterned in a 150 nm thick $Al_{0.35}Ga_{0.65}As$ layer. The membranes were transferred to a transparent gel with a refractive index of 1.4.[12] The composition of the $Al_{0.35}Ga_{0.65}As$ membrane creates a structure that is optically transparent at the SH wavelength of 767.5 nm. To avoid the possibility of a zero effective non-linearity, the photonic and electronic lattices of $Al_{0.35}Ga_{0.65}As$ are misaligned by ~22.5°. Transmission spectra of the membranes are measured as a function of angle of incidence using a 100 μm spotsize on the sample. The transmitted light is collected by a lens into a 400 μm multi-mode fiber connected to spectrometers to cover the spectral range of 400–1700 nm. Apertures placed in the beam limit the numerical aperture to ~0.01. Polarizers are placed in the incident and transmitted beam to control the polarization of the light.

Figure 1 shows a grayscale plot of the measured transmission as a function of the angle of incidence and dimensionless frequency (vertical axis). Data are shown for *s*-polarized light as a function of the dimensionless in-plane wavevector $k_{//}$ along the (1,1) or ΓM direction. The transmission spectra contain a number of asymmetric resonant features that are visible in the figure as the dark and bright lines on top of a slowly varying background. The origin of these features is the coupling of incident light to a guided mode of the slab via diffraction from the periodic lattice of holes.[13,18,19] For comparison, the lines in the figure show a calculation of the photonic band-structure using a finite-difference-time-domain method[20] and literature values of the frequency dependent dielectric constant of the $Al_{0.35}Ga_{0.65}As$ layer.[21,22] The red lines refer to "E"-polarized or *even* modes, while blue lines refer to "H" polarized or *odd* modes. The total transmission is the result of interference between a non-resonant transmission through the $Al_{0.35}Ga_{0.65}As$ layer and a resonant contribution resulting in an asymmetric Fano lineshape with resonant frequency ν, and linewidth Γ.[13,23]

[a]Current address: Cosine Research B.V., Niels Bohrweg 11, 2333 CA Leiden, The Netherlands.
[b]Author to whom correspondence should be addressed. Electronic mail: dood@physics.leidenuniv.nl.

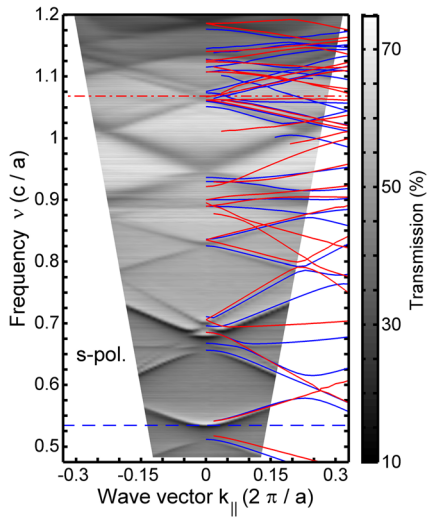

FIG. 1. Measured linear transmission of the two-dimensional photonic crystal, for s-polarized light as a function of the in plane wavevector along the ΓM direction (horizontal axis) and the dimensionless frequency (vertical axis). The lines superimposed on the right hand side of the figure refer to the calculated bandstructure.

Figure 2 shows the measured transmission (open circles) for s-polarized light as a function of the dimensionless frequency for normal incidence (Fig. 2(a)) and an angle of incidence of 10° (Fig. 2(b)). At normal incidence, the structure is resonant at the laser frequency, indicated by the vertical dashed line. For oblique angles of incidence, two resonances are clearly visible. The low frequency resonance is absent at normal incidence (see Fig. 1) and shifts to the red with increasing angle. The higher frequency resonance is resonant with the laser at normal incidence and shifts to the blue with increasing angle of incidence. The solid lines through the data are obtained by fitting a Fano lineshape to the transmission data, defined by

$$T(\nu) = \left| a_{nr} + \sum_{i=1,2} \frac{a_i\, e^{i\varphi}}{i + (\nu - \nu_i)/\Gamma_i} \right|^2 . \qquad (1)$$

Here, a_{nr} represents a non-resonant background corresponding to direct transmission through the thin $Al_{0.35}Ga_{0.65}As$ layer. Each resonance has an amplitude a_i, frequency ν_i, and linewidth Γ_i. Because the slab is placed on a gel substrate, an additional phase φ between the direct and resonant transmission channels should be introduced.[14] All data can be fit satisfactorily by setting $\varphi = 0.33 \pm 0.02$ rad. From the fit, we find the resonant frequency $\nu_2 = 0.53455 \pm 5 \times 10^{-5}\ c/a$ and the quality factor of the resonance $Q_2 = \nu_2/(2\,\Gamma_2) = 100 \pm 5$ at normal incidence. At 10° angle of incidence, we find somewhat lower quality factors $Q_1 = Q_2 = 70 \pm 5$ for the two modes.

To understand measured SH signals as a function of the angle of incidence, it is essential to understand the frequency detuning of the photonic crystal mode relative to the laser frequency. The 150 nm $Al_{0.35}Ga_{0.65}As$ layer acts as a single mode waveguide at 1.5 μm wavelength, with an effective refractive index of the layer below that of bulk $Al_{0.35}Ga_{0.65}As$ due to the presence of the holes. The dispersion relation of the waveguide $\beta(\omega)$, can be found using standard methods.[24] The periodic lattice of holes modifies this dispersion relation via diffraction, which allows adding a reciprocal lattice vector $\vec{G}$

$$\vec{k}(\omega) = \vec{\beta}(\omega) + \vec{G}, \qquad (2)$$

and provides a good approximation of the dispersion away from the stopgaps.[25] Figure 3 shows the frequency of the two lowest resonances in the transmission spectra as a function of the in-plane wavevector $k_{//}$ along the ΓM direction. Data are shown for *s*-polarized (solid symbols) and *p*-polarized light (open symbols) and show clear avoided crossings

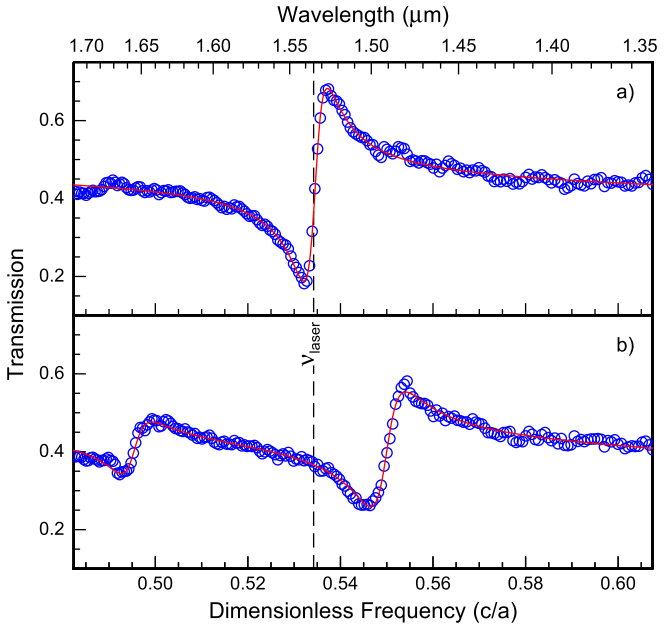

FIG. 2. Measured transmission (symbols) as a function of dimensionless frequency for normal incidence (a) and for an angle of incidence of 10° (b). The lines through the data are fits to a Fano model (see text). The vertical dashed line indicates the laser frequency used for second harmonic generation.

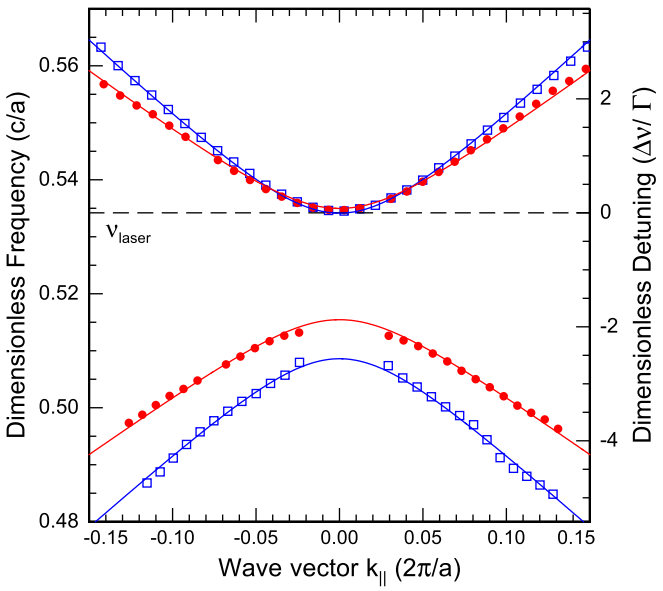

FIG. 3. Dispersion diagram for the lowest order resonances along the ΓM direction. The data show an avoided crossing for both *s*-polarized (open symbols) and *p*-polarized radiation (solid symbols). The right axis indicates a dimensionless detuning for *s*-polarized light, i.e., measured in units of the linewidth of the mode.

centered around a frequency of 0.52 c/a of the fundamental TE waveguide mode folded to the zone center by the $(0,\pm1)$ and $(\pm1,0)$ reciprocal lattice vectors.

The uncoupled modes have frequencies $\nu_{1,2}$, given by

$$\nu_{1,2} = \nu_0\sqrt{\left(1\pm\left(\frac{\alpha k_{//}}{\sqrt{2}}\right)\right)^2+\left(\frac{\alpha k_{//}}{\sqrt{2}}\right)^2}, \qquad (3)$$

where $\nu_0 = (n_{eff})^{-1}$ is the center frequency, with n_{eff} the effective (phase) index of the waveguide mode. The group index of the waveguide mode is given by $n_g = n_{eff}/\alpha$. The holes in the photonic crystal slab couple the modes and create an avoided crossings with frequencies split by an amount $\Delta\nu$ centered around ν_0. We find $\nu_0 = 0.5214 \pm 0.0001\ c/a$ ($n_{eff} = 1.918 \pm 0.001$) and $\Delta\nu/\nu_0 = 4.9\% \pm 0.1\%$ for s-polarized light, and $\nu_0 = 0.5252 \pm 0.0001\ c/a$ ($n_{eff} = 1.904 \pm 0.001$) and $\Delta\nu/\nu_0 = 3.7\% \pm 0.1\%$ for p-polarized light. From the fitted values of α, we deduce group indices $n_g = 5.20 \pm 0.03$ and 6.58 ± 0.03 for s- and p-polarized light, respectively.

SH experiments are done using an Er-Yb based, laser (Cobolt Tango) emitting pulses of 3.8 ns duration at a 5 kHz repetition rate and a 10 mW average power. The laser has a center wavelength of 1535 nm ($\nu = 0.5342\ c/a$) and a narrow linewidth below 0.04 nm. The laser beam is collimated to a 3 mm diameter beam with a corresponding diffraction limited half-angular width of 1 mrad. The SH signal is measured in transmission through a 800 nm shortpass and a 766.5 nm, 25 nm FWHM bandpass filter. The signal is collected by a lens and focused onto an area of $\sim 30 \times 30$ pixels of a cooled CCD camera (Apogee Alta U1). The exposure time is varied from 1 s to 1800 s to create a large dynamic range.

Figure 4 shows the measured SH signal as a function of the in plane wavevector $k_{//}$ along the ΓM direction (bottom axis) and the angle of incidence (top axis). Clear peaks in the signal can be identified at normal incidence and at $k_{//} = -0.378$. In between these peaks, between $k_{//} = -0.2$ and -0.3, a measured background signal of $\sim 6.8 \pm 0.1$ cts/s remains that is related to the nonlinear response of the thin $Al_{0.35}Ga_{0.65}As$ membrane. The peaks are due to a resonant enhancement of the SH signal by the photonic crystal. At normal incidence, the measured peak value is $72\,100 \pm 300$ cts/s, corresponding to an enhancement by a factor 10^4. To connect the measurement in Figure 4 to the measured linear optical properties, we consider the SH generation as a three-step process: (i) external radiation couples to the photonic crystal, (ii) the field inside the photonic crystal generates a non-linear polarization that acts as a source for SH radiation, and (iii) the SH couples to external radiation. The process is considered to be efficient if the coupling of SH to external radiation leads to constructive interference, a condition often referred to as phase-matching. This phase-matching condition is equivalent to a double resonance condition where a resonance occurs at the fundamental wavelength and at the SH wavelength simultaneously.[15]

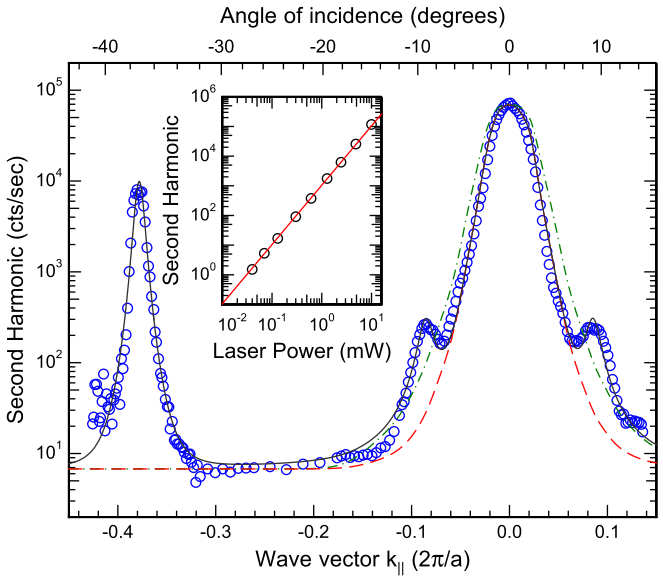

FIG. 4. Measured SH signal of the $Al_{0.35}Ga_{0.65}As$ photonic crystal slab as a function of the in plane wavevector along the ΓM direction (symbols). The corresponding angle of incidence is plotted on the top axis. At normal incidence, the SH is enhanced by 4 orders of magnitude relative to the background. The lines through the data correspond to different models used to explain the data (see text). The inset shows the measured second harmonic intensity as a function of laser power on a log-log scale. The straight line through the data corresponds to a quadratic dependence.

We use the Fano model to quantify the field coupled into the photonic crystal slab and the resonant enhancement. For a narrow line laser, with a frequency spread that is much smaller than the linewidth of the resonance, the pump field coupled into the slab is given by

$$E_P(k_{//}) = E_0\frac{\Gamma}{\left(\nu(k_{//})-\nu_L\right)+i\Gamma} = E_0\frac{1}{i+\left(\Delta\nu(k_{//})/\Gamma\right)}, \qquad (4)$$

where E_0 is the field strength of the incident external field, and $\Delta\nu(k_{//})/\Gamma$ is a dimensionless detuning. This quantity is plotted in Fig. 3, right axis, using the value of Γ determined from the Fano fit of the resonance at normal incidence (see Fig. 2). The SH intensity for a single resonant mode or cavity is given by the square of the intensity at the fundamental frequency[8,9] and is therefore proportional to

$$I_{SH}(k_{//}) \propto d_{eff}^2 E_0^4\left(\frac{1}{1+\left(\Delta\nu(k_{//})/\Gamma\right)^2}\right)^2, \qquad (5)$$

where d_{eff} is an effective non-linearity of the $Al_{0.35}Ga_{0.65}As$ material. For III-V materials, the $\bar{4}3m$ point symmetry of the electronic lattice creates non-zero components d_{xyz} SH, where the labels xyz refer to a Cartesian coordinate system aligned with the electronic lattice of the $Al_{0.35}Ga_{0.65}As$. The incident s-polarization couples to the TE waveguide mode and creates a field with non-zero field components in the x and y directions due to the 22.5° misalignment of the electronic and photonic lattices. The SH field is generated in the z-direction and is expected to couple to TM waveguide modes.

The model as presented by Eq. (5) can be compared to the data directly, using the measured frequency difference relative to the laser frequency $\Delta\nu(k_{//})$. The result is shown in Fig. 4 by the dashed-dotted line and fails to describe the data. The single resonant model of Eq. (5) predicts a feature

that is significantly broader than our measurements. The model can be fit to the data by using Γ as a fitting parameter, resulting in the dashed line in Fig. 4. The quality factor $Q = 145 \pm 5$ derived from this fit is significantly higher than the quality factor $Q = 100 \pm 5$ obtained from the Fano fit in Fig. 2. We interpret the narrower peak in the SH as the result of a resonant coupling to a leaky mode at the SH wavelength. At normal incidence, the double resonance ensures that the radiation is efficiently coupled to the far-field. When the angle is tuned, the resonance at the fundamental and the SH frequency are detuned simultaneously. This leads to a narrower peak that can be described by Eq. (5) if we assume a higher Q to incorporate the detuning at the SH frequency. We measured the resulting second harmonic to be elliptically polarized at normal incidence. This can be explained by imperfections in the structure that break the perfect mirror symmetry of the lattice required for a well-defined output polarization at normal incidence.

Additional support for double resonant conditions is provided by the weak satellite peaks in Fig. 4 that do not relate to a feature in transmission measurements at the laser frequency. The origin of these satellite peaks can only be explained by leaky modes at the SH frequency. From a fit with additional Lorentzian features, as shown by the solid line in Fig. 4, we obtain $k_{//} = \pm 0.085\ 2\pi/a$ and a width $\Delta k_{//} = 0.008\ 2\pi/a$. The second peak at $k_{//} = -0.378\ 2\pi/a$ is a single resonant feature and can be fit by using Eq. (5) with a width $\Delta k_{//} = 0.007\ 2\pi/a$. This resonance is a leaky mode that couples to the laser radiation via a reciprocal lattice vector in the ΓM direction. From the experimental data, we estimate a quality factor of 210 ± 20 of this mode. Using the phase and group velocity of the waveguide, we expect this resonance to occur at $k_{//} = \pm 0.379\ 2\pi/a$, in perfect agreement with measurements.

In conclusion, we have shown that the measured SH signal generated by a two-dimensional photonic crystal slab is enhanced by 4 orders of magnitude. This large enhancement is measured in transmission and at normal incidence, for a photonic crystal slab transferred to a gel substrate. The measured enhancement can be explained by a double resonant condition, where both the pump laser and the SH radiation are resonant with a leaky mode of the photonic crystal. We present a relatively simple model to understand the resonance conditions of the leaky modes and apply this model to SH generation. The benefit of this model over numerical methods, such as finite-difference-time-domain simulations or calculations of Green's functions, is that it allows to insert measurable parameters such as the resonance frequency and quality factor of the resonance directly into the model.

We would like to thank Eduard Driessen and Eric Eliel for stimulating discussions. The photonic crystals in this study were fabricated in the Nanofacility of the Kavli Nanolab at the Delft University of Technology. This research was made possible by financial support from the Dutch Association for Scientifc Research (NWO) and the Foundation for Fundamental Research of Matter (FOM).

[1]J. P. Mondia, H. M. van Driel, W. Jiang, A. R. Cowan, and J. F. Young, Opt. Lett. **28**, 2500 (2003).
[2]A. M. Malvezzi, G. Vecchi, M. Patrini, G. Giuzzetti, L. C. Andreani, F. Romanato, L. Businaro, E. Di Fabrizio, A. Passaseo, and M. De Vittorio, Phys. Rev. B **68**, 161306 (2003).
[3]T. Ishihara and K. Koshino, Phys. Rev. Lett. **91**, 253901 (2003).
[4]G. Vechhi, J. Torres, D. Coquillat, and M. Le Vassor d'Yerville, Appl. Phys. Lett. **84**, 1245 (2004)
[5]J. Torres, D. Coquillat, R. Legros, J. P. Lascaray, F. Teppe, D. Scalbert, D. Peyrade, Y. Chen, O. Briot, M. Le Vassor d'Yerville, E. Centeno, D. Cassagne, and J. P. Albert, Phys. Rev. B. **69**, 085105 (2004).
[6]M. W. McCutcheon, G. W. Rieger, I. W. Cheung, J. F. Young, D. Dalacu, S. Frederick, P. J. Poole, G. C. Aers, and R. L. Williams, Appl. Phys. Lett. **87**, 221110 (2005).
[7]M. W. McCutcheon, J. F. Young, G. W. Rieger, D. Dalacu, S. Frederick, P. J. Poole, and R. L. Williams, Phys. Rev. B. **76**, 245104 (2007).
[8]K. Rivoire, Z. Lin, F. Hatami, W. T. Masselink, and J. Vuckovic, Opt. Express **17**, 22609 (2009).
[9]M. Galli, D. Gerace, K. Welna, T. F. Krauss, L. O'Faolain, G. Guizzetti, and L. C. Andreani, Opt. Express **18**, 26613 (2010).
[10]A. D. Bristow, J. P. Mondia, and H. M. van Driel, J. Appl. Phys. **99**, 023105 (2006).
[11]M. J. A. de Dood, W. T. M. Irvine, and D. Bouwmeester, Phys. Rev. Lett. **93**, 040504 (2004).
[12]W. T. M. Irvine, M. J. A. de Dood, and D. Bouwmeester, Phys. Rev. A **72**, 043815 (2005).
[13]G. Weihs, Int. J. Mod. Phys. B **20**, 1543 (2006).
[14]Lj. Babić, R. Leijssen, E. F. C. Driessen, and M. J. A. de Dood, Opt. Express **19**, 19532 (2011).
[15]S. Fan, W. Suh, and J. D. Joannopoulos, J. Opt. Soc. Am. A **20**, 569 (2003).
[16]Lj. Babić and M. J. A. de Dood, Opt. Express **18**, 26569 (2010).
[17]A. R. Cowan and J. F. Young, Phys. Rev. B **65**, 085106 (2002).
[18]M. Kanskar, P. Paddon, V. Pacradouni, R. Morin, A. Busch, J. F. Young, S. R. Johnson, J. MacKenzie, and T. Tiedje, Appl. Phys. Lett. **70**, 1438 (1997).
[19]V. N. Astratov, D. M. Whittaker, I. S. Culshaw, R. M. Stevenson, M. S. Skolnick, T. F. Krauss, and R. M. De La Rue, Phys. Rev. B **60**, R16225 (1999).
[20]A. F. Oskooi, D. Roundy, M. Ibanescu, P. Bermel, J. D. Joannopoulos, and S. G. Johnson, Comput. Phys. Commun. **181**, 687 (2010).
[21]D. E. Aspnes, S. M. Kelso, R. A. Logan, and R. Bhat, J. Appl. Phys. **60**, 754 (1986).
[22]P. G. Snyder, J. A. Woollam, S. A. Alterovitz, and B. Johs, J. Appl. Phys. **68**, 5925 (1990).
[23]U. Fano, J. Opt. Soc. Am. **38**, 921 (1948).
[24]P. Yeh, *Optical Waves in Layered Media* (Wiley, New Jersey, 1998).
[25]K. Sakoda, *Optical Properties of Photonic Crystals* (Springer, Berlin, 2001).